4

Recent Developments of ENDOR Spectroscopy in the Study of Defects in Solids

BY J.-M. SPAETH

1. Introduction

Point defects such as impurity atoms or ions or intrinsic defects such as vacancies, interstitials or anti-site defects in binary crystals or aggregates of these defects very often determine the bulk properties of a solid. This is the case in, e.g., ionic crystals or oxides and is particularly important technologically in semiconductors. Therefore it is of prime interest for materials science to have methods that are able to determine the defect structures. Radiation damage to solids and detection of ionising radiation are other fields where knowledge of the structures of the defects created and their interactions is absolutely necessary.

Magnetic resonance is the most powerful technique for determining defect structures of point defects. Electron spin resonance (ESR) is a widespread method, but unfortunately suitable only in particularly favourable cases. It turns out that a combination of electron spin resonance and nuclear magnetic resonance, electron nuclear double resonance (ENDOR), is the most powerful tool, provided it works for the specific defect under investigation. In cases of interest to materials science, ENDOR spectra are mostly very complicated. This may be the reason why ENDOR spectroscopy in solids has not become more popular. Computer assisted experiments and analysis of spectra have, however, together with advanced ENDOR methods, made ENDOR spectroscopy in recent years quite feasible and of practical use beyond simple model cases, for which this spectroscopy was originally applied following its discovery in 1959.[1]

The aim of this Chapter is to described briefly the present possibilities of ENDOR spectroscopy for investigating point defects in solids. It is attempted to discuss and illustrate what can be done without going into great detail, especially with respect to a precise analysis of the spectra, which would be beyond the scope of this Chapter. The examples used to illustrate the methods are, for convenience, largely taken from recent work of the Paderborn group. Therefore, this is not a review article in the sense of summarising

all work done in the field. It is furthermore assumed that the reader is familiar with the basic concepts and the realisation of electron spin resonance which will not be discussed. The fundamental ideas of ENDOR will be briefly described as well as the basic methods of analysing ENDOR spectra.

This article does not deal with the possibility of measuring ENDOR using electron spin echo methods. These methods have certain advantages, especially at low frequencies, but have also serious disadvantages, in particular in the regime of broad ESR lines and high ENDOR frequencies. The reader is referred to recent articles by Schweiger for these experimental methods.[2]

2. Structure Determination of Defects by Magnetic Resonance

The possibility of determining defect structures by magnetic resonance spectroscopy is based on the measurement of the magnetic interaction between the magnetic moment of the unpaired electron(s) or hole(s) of the defect and the magnetic moments of nuclei belonging to the 'impurity' atom of the defect (if any) and the atoms of its surrounding lattice. This interaction is usually called hyperfine (hf) interaction if it occurs between the unpaired electron (hole) and the central nucleus of an impurity atom, if such a defect is under study, and it is called superhyperfine (shf) interaction or ligand hyperfine (lhf) interaction if it occurs between the magnetic moment of the unpaired electron (hole) and the magnetic moments of the nuclei of the surrounding lattice. In Figure 1 a schematic representation of a defect is shown, in which the electron spin and the nuclear spins are indicated. The hf interaction is often resolved in ESR and if the impurity nucleus occurs in several magnetic isotopes then a chemical identification of the impurity is easily possible by taking advantage of the known magnetic moments, the ratio of which determines the ratio of the observed hf splittings (see below) and by measuring the ESR signal intensities, which reflect the natural abundance of the different isotopes. Unfortunately there are important and common impurities, like oxygen, where over 99% of the isotopes are non-magnetic. In such a case, a specific doping of a magnetic isotope (e.g., ^{17}O) may be necessary.

The g-factors (g-tensors) of the ESR spectra contain also information on the defect structure, mainly on its symmetry. For a precise structure determination, apart from symmetry, the g-factor analysis usually does not yield enough reliable information, since excited state energies are involved in the g-factor analysis, which

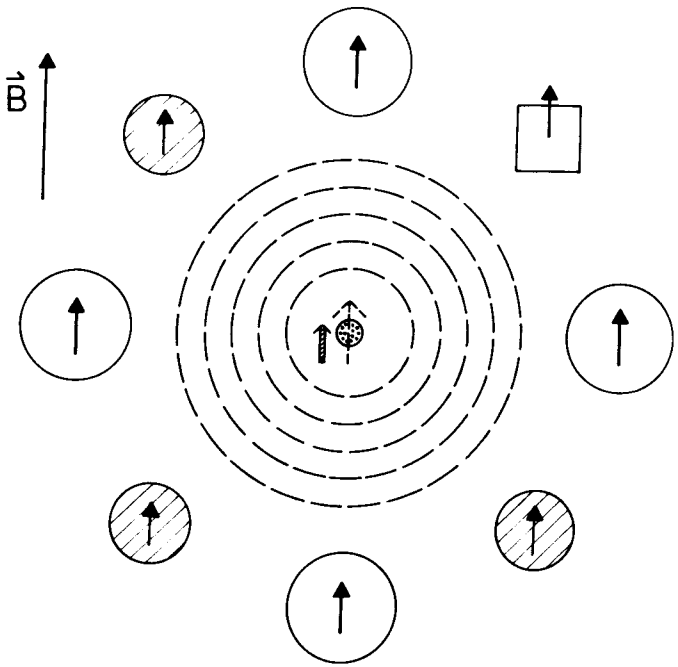

Figure 1 *Schematic representation of a defect in a solid. The unpaired electron spin, the electron spin density distribution and the nuclear spins of the lattice nuclei are indicated*

are mostly not known.[3-5]

If it were possible to measure the nuclear magnetic resonance (NMR) of the nuclei of the surrounding lattice, the local magnetic fields seen by the nuclei would just give the required information on the defect structure, since it is a superposition of the applied static magnetic field and the field equivalent of the shf or lhf interactions. If the local fields of all the nuclei were known together with their symmetry relation to the defect site, the structure of the defect including the presence of vacancies and lattice distortions could be derived. Unfortunately, however, NMR is not sufficiently sensitive. One needs at least about 10^{19} nuclei like protons to measure NMR, while one deals with defect concentrations of 10^{16} cm^{-3} and less and sample volumes usually well below 1 cm^3.

In ESR the shf is mostly not well resolved. If at all it is resolved usually only with the nearest neighbour nuclei. Therefore,

ESR spectroscopy is often suitable for inpurity identification by a resolved hf interaction, but not for a precise microscopic structure determination. In fact, recently in GaAs several ESR spectra were observed with the same central ^{75}As hf splitting and almost the same line width, which all belong to different defect structures. These different defects have only one common feature; an arsenic antisite, i.e., an arsenic atom on a Ga-site is involved. However, the rest of the structure is different.[6] By measuring only ESR one can be badly misled.

A higher resolution for the shf interactions and a higher sensitivity than obtained in NMR is achieved by measuring ENDOR.[1] The NMR transition of neighbour nuclei coupled to the unpaired electron causes a change of the electron spin polarisation under suitable experimental conditions (partly saturated ESR), which can be detected as ENDOR signals (see below). Thus, the NMR transitions are detected using a quantum transformation to higher quanta, the ESR microwave quanta, which results in a higher sensitivity.

It must be noted that by resolving the shf interactions and the ligand quadrupole interactions one can determine the number and the symmetry relation of neighbour nuclei with respect to the defect centre and also the coupling constants such as shf and quadrupole constants. It is not, however, possible to determine from the coupling constants the distance of the identified nuclei from the defect centre without having a theoretical wave function for the defect electron (hole) or without assumptions about the radial part of this wave function, e.g., whether it falls off monotonously with distance from the defect core. This is very often the case but not always. Especially for shallow defects in semiconductors there may be oscillations of the unpaired spin density with distance. If a reasonable assumption about this radial part can be made, then a clear defect model can be derived unless there are special symmetry conditions in which one cannot decide between possible sites. This is, e.g., the case for the substitutional and the tetrahedral interstitial site in the diamond structure. There the same symmetry type of neighbour nuclei occurs, only with a different sequence. If nothing is known about the wave function, one cannot decide on the site from ENDOR alone. Such a case occured for instance recently for chalcogen defects in silicon.[7]

3. Hyperfine and Superhyperfine Structure of ESR Spectra

ESR lines can be split by hyperfine (hf) and superfine (shf) interactions. It is this splitting which gives most information on

the microscopic nature of the defects in ESR. The hf and shf interactions are described by the respective hf (shf) tensors A and the spin Hamiltonian

$$H = g_e\beta_e\vec{B}_0\vec{S} + \sum_i(\vec{I}_i\tilde{A}_i\vec{S} - g_{I,i}\beta_n\vec{B}_0\vec{I}_i) \qquad (3.1)$$

The sum runs over all nuclei with which the shf (hf) interaction is measured. g_e is the electronic g-factor, β_e the Bohr magneton, β_n the nuclear magneton and g_I the nuclear g-factor.

For the simple case of an isotropic g-factor, S = 1/2 and for only one nucleus interacting in perturbation theory of first order one obtains for the ESR transitions frequencies:

$$h\nu_{ESR} = g_e\beta_e B_{res} + m_I A(\theta) \qquad (3.2)$$

where $A(\theta)$ denotes that the hf interaction is in general angular dependent, i.e., it depends on the relative orientation of the external magnetic field and the principal axes of the hf tensor.

For the simple case of I = 1/2 there are two values of the nuclear spin quantum number $m_I = \pm 1/2$. Since in the experiment ν_{ESR} is kept constant, there are two resonant fields, which are separated by $A(\theta)/g_e\beta_e$.

Figure 2 shows how an hf interaction can be used for defect identification for the example of Te^+ defects in Si.[8] 92% of the Te isotopes are diamagnetic and give rise to the central ESR line near 3500 G (measured in X-band) corresponding to $g_e = 2$. The two magnetic isotopes ^{125}Te (7% abundant) and ^{123}Te (0.9% abundant) both have I = 1/2 and according to equation (3.2) a doublet splitting. The ESR line intensities follow the isotope abundance and the relative splittings are in the ratio of the respective nuclear moments (see below). Therefore the defect is unambiguously identified as being due to Te impurities. However, no further structure due to the shf interactions is resolved. Therefore, the site of Te^+ in the lattice cannot be determined from ESR.

Figure 3 shows the ESR spectrum of atomic hydrogen on interstitial sites, and on cation and anion vacancy sites in KCl.[9] The central hf splitting with the proton (I = 1/2) is in all three cases practically the same and nearly that of the free hydrogen atom. Only for the interstitial site is a shf interaction with nearest neighbours resolved. The substitutional sites cannot be inferred from the ESR spectrum. They could be established only by resolving the shf interactions with ENDOR experiments.[10]

The intensity ratio of the shf lines is a characteristic feature

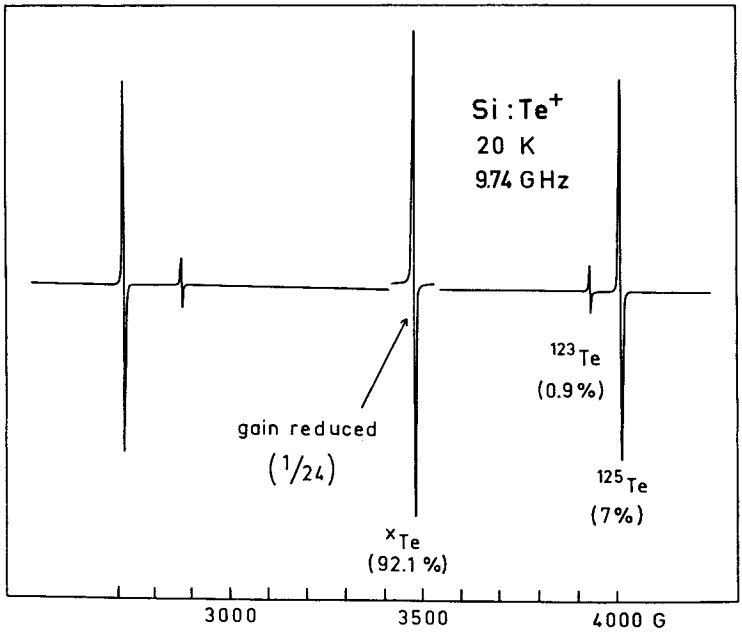

Figure 2 *ESR spectrum of Te^+ centres in Si. The g-factor is isotropic. The hf splittings are due to the two magnetic isotopes ^{125}Te and ^{123}Te with I = 1/2. (After ref. 8)*

and can be used to determine the number of interacting nuclei and their spin. Especially if there are several nuclei with the same shf interaction, which can occur for a specific orientation of the magnetic field, one can define a total nuclear spin N·I, which leads to a (2NI+1) fold splitting of the ESR spectrum. Figure 4 shows the level scheme and the transitions for N = 1, 2 and 3 in the case of I = 1/2. The relative ESR signal height is given by the statistical weights or degeneracy of the levels. For N = 3 they are 1:3:3:1 for the four equidistant shf lines. For four equivalent nuclei of I = 3/2 the weights are 1:4:10:20:31:40:44:40:31:20:10:4:1 for the thirteen shf lines. This is what is observed in Figure 3 for the interstitial atomic hydrogen in KCl, which interacts predominantly with four nearest ^{35}Cl nuclei, which have I = 3/2.

The hf and shf tensors are determined in their principal axis system from an analysis of the angular dependence of the ESR spectra.[3-5]. It is convenient for the discussion below to decompose

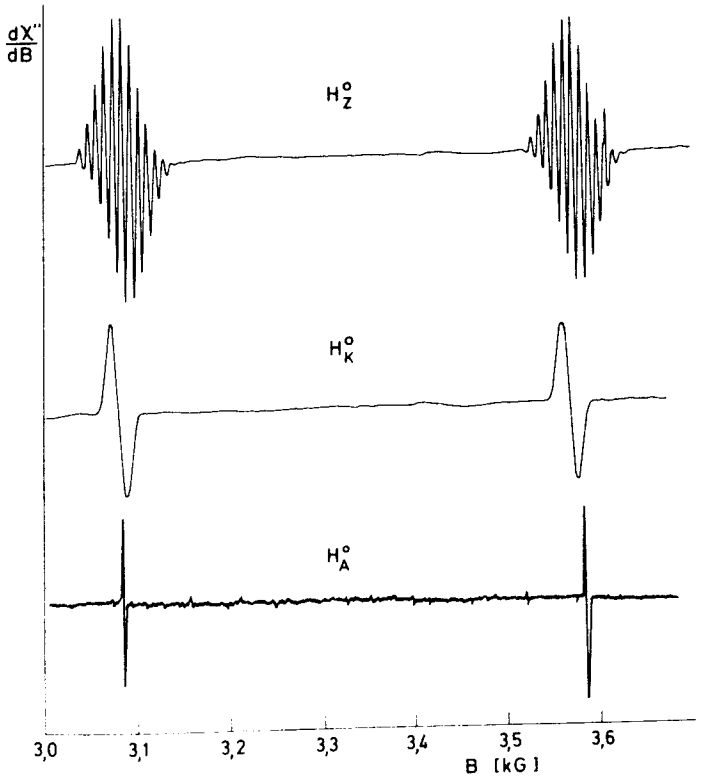

Figure 3 *ESR spectra of three atomic hydrogen centres in KCl. B_0//<100>, T = 77 K. The hydrogen atoms occupy interstitial sites (H_Z^0-centres), cation vacancy sites (H_K^0-centres) and anion vacancy sites (H_A^0-centres). The splitting due to the hyperfine interaction with the proton is almost that of the free hydrogen atom. (After ref. 9)*

the hf (shf) tensors into an isotropic and anisotropic part according to:

$$\tilde{A} = (a \cdot \tilde{I} + \tilde{B}) \tag{3.3}$$

$$b = 1/2B_{zz} \tag{3.4}$$

$$b' = 1/2(B_{xx} - B_{yy}) \tag{3.5}$$

where a is the isotropic hf (shf) constant (Fermi contact term), b is the anisotropic hf (shf) constant and b' describes the deviation of the tensor from axial symmetry. x, y, z is the principal axis

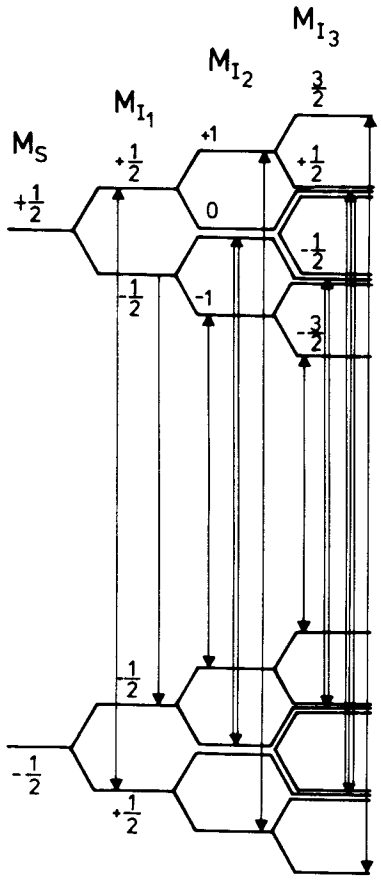

Figure 4 *Electron Zeeman level scheme for an electron with shf coupling to three equivalent nuclei with I = 1/2 and the resulting ESR transitions*

system, whereby the largest interaction is along the z-direction.

A discussion of the interpretation of the hf (shf) interaction is beyond the scope of this Chapter. However, to facilitate understanding of the following discussions some introductory remarks are necessary.[3,4]

The hf interaction constants are determined by the electronic wave function of the defects and the nuclear moments of the nuclei. In a simple one particle approximation the isotropic constant, a, is

given by:

$$a_1 = \frac{2}{3}\mu_0 g_e \beta_e g_I \beta_n |\psi(r_1)|^2 \tag{3.6}$$

where $\psi(r)$ is the wave function of the defect, $\psi(r_1)$ its amplitude at the site r_1 of a particular nucleus. The anisotropic tensor elements are given by:

$$B_{ik} = \frac{\mu_0}{4\pi} g_e \beta_e g_I \beta_n \int (\frac{3}{r^5} x_i x_k - \frac{1}{r^3}\delta_{ik}) |\psi(r)|^2 \, dV \tag{3.7}$$

where r is the radius vector from the nuclear site of concern (origin) where the origin is squared in the integral of equation (3.7). Thus, the hf constants are proportional to g_I and therefore the interaction constants of different isotopes must be in the ratio of their respective g_I factors. This was used for the identification of Te^+ defects in Si.[8]

In solids the shf structure of defects is usually not, or only partly, resolved in ESR. The reason is not because it is too small, but because the ESR spectrum is a superposition of too many shf lines with splittings, which are not very different from each other. In Figure 5 this is schematically shown for a S = 1/2 defect and interactions with two shells of equivalent nuclei, each of which contains n_1 and n_2 nuclei with spin I_1 and I_2, respectively. For both electron Zeeman levels there are $N = (2n_1 \cdot I_1+1)(2n_2 \cdot I_2+1)$ sublevels and therefore there are up to N ESR transitions. If there is no quadrupole interaction, there are, however, only four ENDOR transitions, two for each shell of equivalent nuclei, which follows from the ENDOR selection rules as NMR transitions (see below). Taking into account more interactions, then an exponential increase in the number of superimposed ESR lines results, which are no longer resolved. For solid state defects interactions with up to ten shells of neighbour nuclei are not unusual. What the ESR shows is only the envelope of all the shf transitions yielding an 'inhomogeneously' broadened ESR line. Figure 2 is an example of this; the width of the Te^+ ESR lines is due to unresolved shf interactions with many shells of ^{29}Si nuclei. In ENDOR there are only two lines for each shf coupled nucleus with distinguishable shf interaction (for S = 1/2). In ENDOR there is therefore an excellent resolution of shf interactions.

4. Electron Nuclear Double Resonance (ENDOR)

4.1 Stationary ENDOR - There are two methods of measuring ENDOR, if

one does not include spin echo techniques. The dispersion method is suited for especially long spin lattice relaxation times, T_1. The other is the stationary ENDOR method, which is the more versatile of the two. The former was introduced by Feher,[1] the latter by Seidel.[11]. A quantitative description of both methods is difficult, since for solid state defects the situation is so complicated with regard to relaxation paths and couplings that as yet there is no good general quantitative understanding of the ENDOR effect. Since the purpose of this Chapter is to show the application of ENDOR to

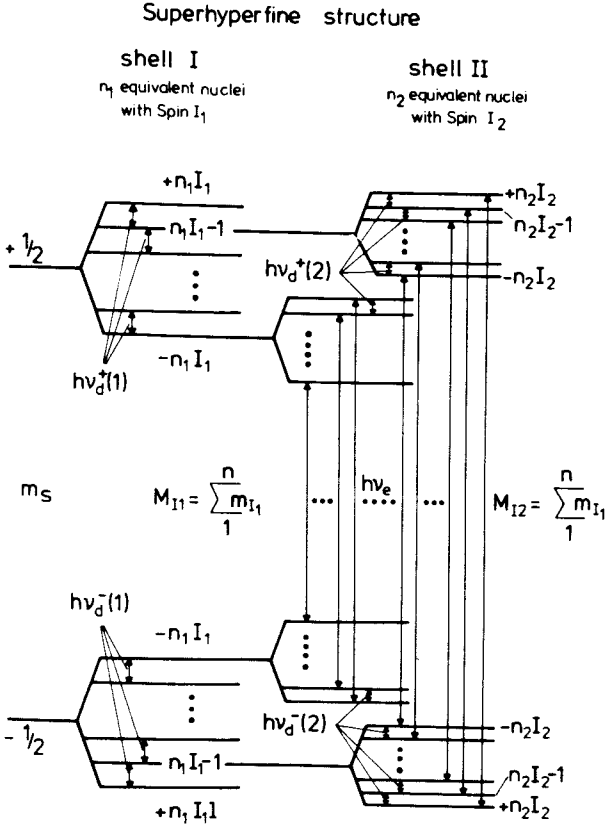

Figure 5 *Electron Zeeman level scheme for an electron with shf coupling to several shells of equivalent nuclei. The ESR line is an envelope over all shf lines, which usually are not resolved any more due to the large number of superimposed lines*

the determination of defect structures, only the more commonly used stationary ENDOR is discussed by means of a simple working model to illustrate the experiments carried out.

Figure 6 shows for S = 1/2 and one nucleus with I = 3/2 schematically the allowed ESR transitions with resolved shf structure. In

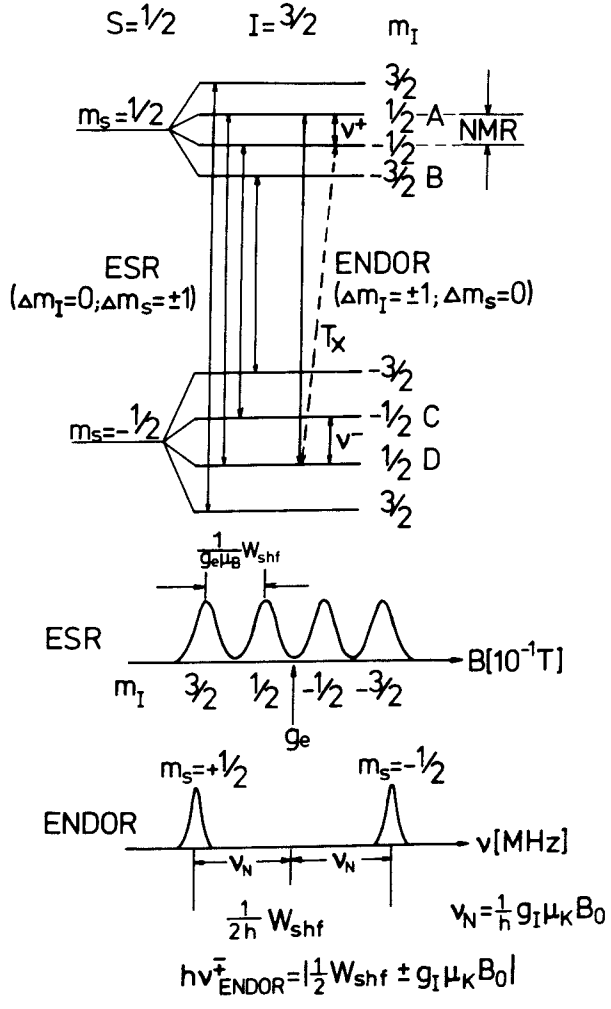

Figure 6 *Energy level diagram to explain stationary electron nuclear double resonance (ENDOR) (see text)*

an ENDOR experiment one of the allowed ESR transitions is partially saturated, that is one chooses a microwave power sufficiently high so that the transitions probability, $W_{MW} = \gamma B_1^2$, is of the order of or larger than the spin lattice relaxation rate, $W_{REL} = 1/T_1$ (γ is the gyromagnetic ratio of the electron and B_1 the microwave field amplitude). If this is the case then the spin population of the levels connected by the microwave transitions deviates from the Boltzmann equilibrium distribution. If $W_{MW} >> W_{REL}$, then these levels become equally populated. This results in a decrease and ultimately disappearance of the observable microwave absorption, since microwave absorption and emission probabilities are equal. The levels not connected by the microwave transitions are not affected. Therefore, e.g., the level population $m_S = +1/2$, $m_I = +1/2$ is now inverted with respect to the level $m_S = +1/2$, $m_I = -1/2$ (see Figure 6). If these two levels are connected by an NMR transition, the level populations can be equalised, which results in a population decrease of the level $m_S = +1/2$, $m_I = +1/2$ leading to desaturation of the (partially) saturated transition $m_S = -1/2$, $m_I = +1/2$ to $m_S = +1/2$, $m_I = +1/2$. This desaturation has been monitored. It occurs for two NMR frequencies in the example in Figure 6 since the NMR frequencies for $m_S = +1/2$ and $m_S = -1/2$ are different (see below). Thus, each nucleus gives rise to two ENDOR lines (for $S = 1/2$). A cross relaxation T_x (see Figure 6) allows the stationary observation of the desaturation (stationary ENDOR).[11] If several nuclei with the same or similar interactions are coupled to the unpaired electron, then the ESR pattern becomes complicated and the shf structure is usually not resolved. In ENDOR all nuclei with the same interaction give rise only to two (for $S = 1/2$) ENDOR lines, which greatly enhances the resolution. ENDOR lines, like NMR lines, are typically 10-100 kHz wide, about three orders of magnitude narrower than homogeneous ESR lines. Thus in ENDOR one uses the sensitivity enhancement due to a quantum shift from frequencies of the order of MHz to the microwave frequencies of the order of GHz and the increased resolution power due to the smaller NMR linewidth and the reduction in the number of lines.

Figure 7 shows as an example ENDOR lines (ESR desaturation) of the nearest ^{19}F neighbours of $F(Cl^-)$ centres in SrFCl (for $m_S = -1/2$), where the unpaired electron occupies a Cl^- vacancy. The structure model of BaFCl, which has the same structure, is contained in Figure 18.

4.2 Analysis of ENDOR Spectra - In general, there is besides the

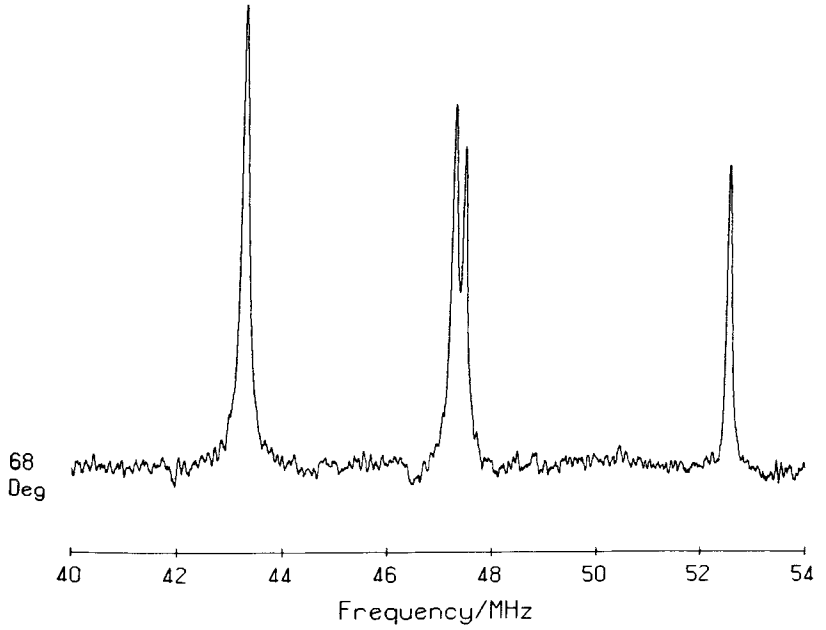

Figure 7 *ENDOR lines due to the nearest ^{19}F neighbours of $F(Cl^-)$ centres in SrFCl*

shf interaction a quadrupole interaction if I>1/2 for the interacting nuclei. This interaction is due to the interaction between the electrical field gradient at the site of a nucleus and its nuclear quadrupole moment. Therefore the spin Hamiltonian describing the ENDOR spectra is:

$$H = g_e\beta_e\vec{B}_0\vec{S} + \sum_i(\vec{S}\tilde{A}_1\vec{I}_1 - g_I\beta_I\vec{B}_0\vec{I}_1 + \vec{I}_1\tilde{Q}_1\vec{I}_1) \qquad (4.1)$$

The sum runs over all nuclei interacting with the unpaired electron. For simplicity it is assumed that g_e is isotropic (which is generally not the case). Q is the traceless quadrupole interaction tensor with the elements

$$Q_{ik} = \frac{eQ}{2I(2I-1)} \quad \frac{\partial^2 V}{\partial x_i \partial x_k}\Bigg|_{r=0} \qquad (4.2)$$

where Q is the quadrupole moment and V the electrical potential. The spectra are usually analysed in terms of the quadrupole interaction constants:

$$q = 1/2Q_{zz}, \quad q' = 1/2(Q_{xx} - Q_{yy}) \tag{4.3}$$

The selection rule for ENDOR transitions , like NMR transitions, is:

$$\Delta m_s = 0, \quad \Delta m_I = \pm 1 \tag{4.4}$$

If the shf and quadrupole interaction is small compared to the electron Zeeman term, then the quantisation of the electron spin is not influenced by these interactions and the nuclei are independent of each other. They can be treated separately and the sum in equation (4.1) can be omitted. In purturbation theory of first order, that is with the conditions

$$B_{ik}, Q_{ik} << a \pm \frac{1}{m_s} g_I \beta_n B_0 \tag{4.5}$$

$$\nu_{ENDOR} = \left| \frac{1}{h} |m_s| W_{shf} \pm \nu_n \pm \frac{1}{h} m_q W_Q \right| \tag{4.6}$$

with the following abbreviations:

$$W_{shf} = a + b(3\cos^2\theta - 1) + b'\sin^2\theta\cos 2\delta \tag{4.7}$$

$$W_Q = 3\, q(3\cos^2\theta' - 1) + q'\sin^2\theta'\cos 2\delta' \tag{4.8}$$

where θ, δ and θ', δ' are the polar angles of B_0 in the principal shf and the quadrupole axis system, respectively.

$$\nu_n = \frac{1}{h} g_I \beta_n B_0 \tag{4.9}$$

where ν_n is the Lamor frequency of a free nucleus in the magnetic field B_0.

$$m_q = 1/2(m_I + m'_I) \tag{4.10}$$

where m_q is the average of the two nuclear spin quantum numbers, which are connected by the transition.

The basic concepts for the analysis of ENDOR spectra will be described assuming that equation (4.6) holds for the frequency positions of the ENDOR lines. This is in general not the case, since both the anisotropic and quadrupole interactions can become too large with resect to the isotropic term and g-anisotropies as well as the fine structure interaction can influence the spectra. A detailed discussion of the complications is beyond the scope of this Chapter. Some particularly important consequences of higher order

contributions to the frequency positions will, however, be discussed below.

Figure 8 shows and ENDOR spectrum of interstitial atomic hydrogen in KCl for $B_0//(110)$, the ESR spectrum of which is shown in Figure 3 [for $B_0//(100)$]. The ENDOR spectrum contains the interaction with the nearest Cl-neighbours.[9] The identification of the chemical nature of nuclei can be achieved in various ways. According to equation (4.6), for S = 1/2 and no quadrupole interactions, each nucleus gives a pair of lines separated by $2\nu_n$ if $1/2W_{shf} > h\nu_n$ and by W_{shf} if $h\nu_n > 1/2W_{shf}$. Since ν_n can be calculated according to equation (4.9), the nuclei can be identified either from the line pairs separated by $2\nu_n$ or by symmetric line patterns about ν_n.

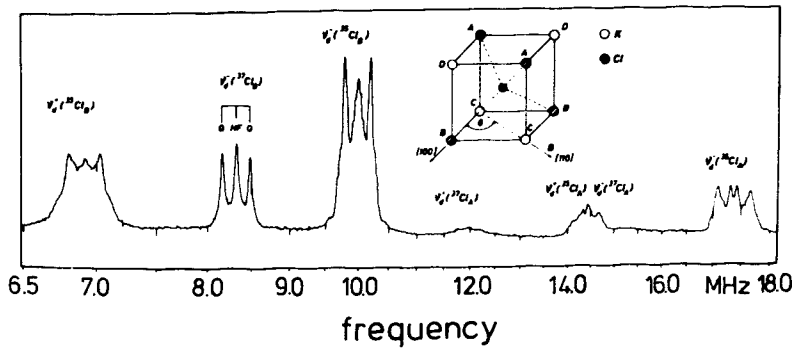

Figure 8 *ENDOR spectrum of the nearest halogen neighbours of interstitial atomic hydrogen centres in KCl.B_0//<100>. (After ref. 9)*

If there are several magnetic isotopes present (such as ^{37}Cl and ^{35}Cl in Figure 8), then their line positions must be in the ratio of their respective nuclear moments (if Q = 0). The line intensity roughly reflects the isotope abundance. Unfortunately, the ENDOR line intensity is very little understood quantitatively in solids due to the many and complicated relaxation paths. Therefore, the two lines according to equation (4.6) of each nucleus cannot always be observed. in particular for low frequencies in stationary ENDOR. However, on shifting the magnetic field through the ESR line the ENDOR line positions are also shifted according to equations (4.6) and (4.9). The ENDOR line shift is due to the shift of ν_n and is thus proportional to g_I, which is characteristic for a particular nucleus. If the ESR linewidth does not allow a big enough ENDOR line shift to be detected (which depends on the ENDOR linewidth), then

one can either do additional experiments with a different ESR band (e.g., K-band or Q-band) or change the resonant frequency of the cavity by inserting material of a suitable dielectric constant and changing the microwave source frequency accordingly.

If there is a quadrupole splitting, then each 'hf' ENDOR line is split into a characteristic multiplet, e.g., for I = 3/2 into a triplet. This is easily recognised in Figure 8 as a triplet structure of each of the ENDOR lines.

In order to determine the defect structure and the interaction parameters, the dependence of the ENDOR line positions upon variation of the magnetic field with respect to the crystal orientation must be measured and analysed. This is the major problem in an ENDOR analysis and the essential tool for the determination of the defect structure.

Figure 9 (a)-(c) show such an angular dependence for a cubic crystal, such as an alkali halide, calculated according to equation (4.6) for the first three neighbour shells of a defect on a lattice site. The patterns are characteristic for (100), (110), and (111) 'symmetry' of the neighbour nuclei. For each m_s value such a pattern is observed. From the number of such patterns, according to equation (4.6) one can infer the electron spin of the defect and thus often its charge state.

Each nucleus has its own principal axis system for the shf and quadrupole tensors. Often, their orientation in a crystal is determined by symmetry. Otherwise, they must be determined from the analysis of the angular dependence of the ENDOR spectra. If the defect centre (impurity) and the respective nucleus are in a mirror plane, then two principal axes must be in this mirror plane. If the connection line between the nucleus and the centre is a threefold or higher symmetry axis, then the tensor is axially symmetric with its axis in this symmetry axis. If the angular patterns are separated in frequency, they are easily recognised and the analysis is fairly straightforward.

Figure 10 shows such an angular dependence for substitutional Te^+ in Si (see Figure 2 for the ESR spectrum). In practice, one proceeds as follows: one assumes a centre model and then calculates the expected angular dependence according to the appropriate spin Hamiltonian making use of the symmetry properties of the assumed model. Comparison with the experimental angular dependence then shows this assumption to be true or false. The symmetry patterns of the neighbour cells may not be easily recognised, if the first order solution of the Hamiltonian is not sufficient. For the tetrahedral

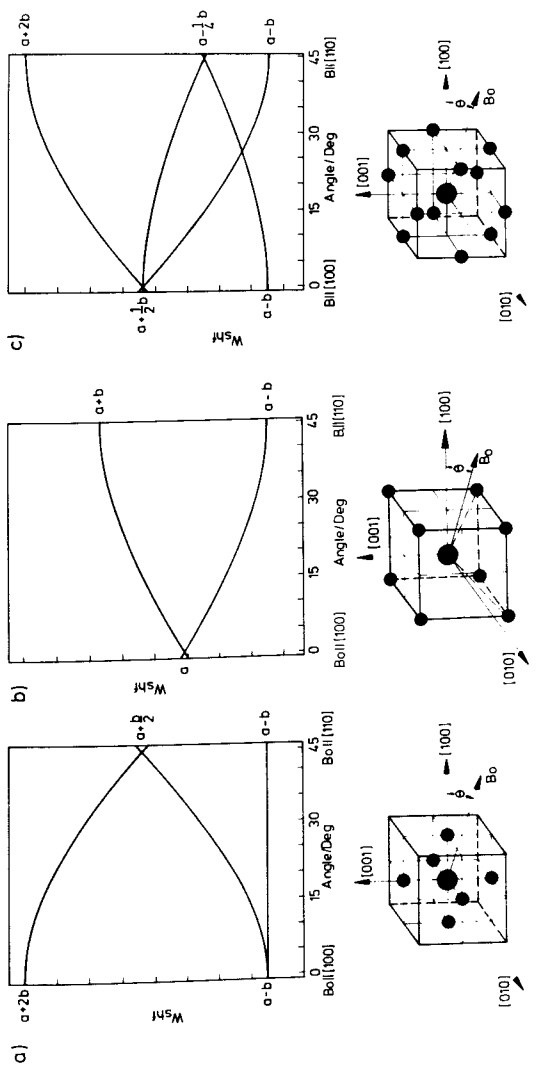

Figure 9 *Calculated ENDOR angular dependence for a defect on a cation substitutional site. (a) (100)-neighbours, (b) (111)-neighbours, (c) (110)-neighbours*

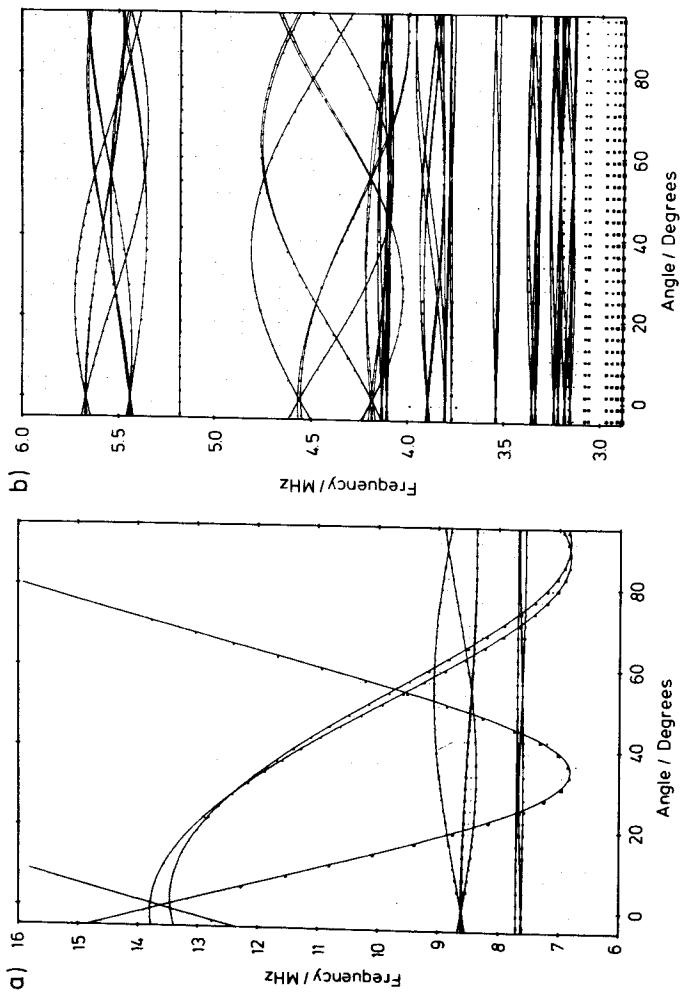

Figure 10 *Angular dependence of ^{29}Si ENDOR lines of Te^+ defects in Si for rotation of the magnetic field in a (110) plane. 0° = <100>. The solid lines are the calculated angular dependencies with the parameters of Table 3. (After ref. 12)*

symmetry of a substitutional point defect in a diamond lattice or zincblende lattice, the shf interactions of nearest neighbours should give the simple pattern of Figure 11. If I = 3/2 for the nearest neighbours and a small quadrupole interaction is present, the pattern looks like Figure 11(b), where the quadrupole triplet splitting of the ENDOR lines is easily recognised. However, for larger values of the quadrupole interaction constant, q, after diagonalisation of the spin Hamiltonian the pattern changes considerably [Figure 11(c)] and its origin is not so easily recognised. It is often this complication through quadrupole interactions that makes the analysis difficult.

In the case of the diamond or zincblende structure (silicon or III-V compounds) there is the particular difficulty in that the symmetry of the substitutional site and tetrahedral interstitial site cannot be distinguished as to the symmetry type of neighbour nuclei with respect to both defects. There are neighbours with (100), (110), and (111) symmetry of their tensors, only the sequence is different in each case. From experiment only the symmetry type of nuclei can be determined, not the distance of the nuclei from the defect core. Here theoretical arguments about the site of the defect or the character of the wave function must be taken into account before establishing a definite model.[12,13]

If the agreement between the calculated angular dependence and the experimental one is good, the analysis is unambiguously correct. There are many more experimental data than parameters to be extracted from them. As an example of the result of such an analysis, Table 1 gives the shf and quadrupole interaction constants of atomic hydrogen on anion sites in KCl($H^0_{s,a}$ centres).[10] The analysis unambiguously the site for the hydrogen atom from the symmetry of the neighbour nuclei. The shf and quadrupole interaction constants could be determined down to vary small interactions with high precision. The spin Hamiltonian has to be diagonalised numerically.[10,14] Another example is that of Te^+ in Si (Table 2). Here the sequence of Si neighbours is classified according to their symmetry types. As mentioned above, only theoretical arguments lead finally to an unambiguous assignment of the Te^+ to the substitutional site.[13]

In a straight ENDOR analysis only the relative signs of the shf constants a, b, b' can be determined and also not the signs of the quadrupole interaction constants with respect to the shf interaction constants. With ENDOR-induced ESR and DOUBLE-ENDOR more can be extracted from experiment about the signs of the interactions.

In solids a particular situation is met, if there are shf (and

Table 1 *Shf and quadrupole constants of $H^0_{S,a}$-centres in KCl (in kHz), T = 40 K**

Shell	*Constant*	$H^0_{S,a}$
$^{39}K_I$	a	253
	b	219
	q	198
$^{35}Cl_{II}$	a	57
	b	312
	b'	-3
	q	-88
	q'	-94
$^{35}Cl_{IV}$	a	37
	b	54
	q	±45
$^{39}K_V$	a	4
	b	11
	b'	~ 0
	Φ_3	26.0° ± 0.2°
	q	±39
	q'	±17
	Φ_Q	13.5° ± 0.2°

*After ref. 10.

Table 2 *Shf interactions of the Te^+ and S^+ centres with ^{29}Si**

Type	*Si:Te⁺* *a/MHz*	*b/MHz*	*b/MHz*	Θ_{shf}	*Si:S⁺* *a/MHz*	*b/MHz*
111	17.7	9.8			32.7	12.0
	11.4	0.47			9.0	0.62
	1.3	0.03			2.94	0.02
100	4.6	<0.005	<0.005		2.04	0.05
	1.8	0.02	<0.005			
110	2.83	0.51	-0.08	53.1	8.94	0.47
	5.26	0.21	0.12	67.1	3.84	0.42
	9.52	-0.09	-0.03	0	4.77	0.03
	1.95	0.1	0.02	-5		
	2.46	0.04	<0.005	50.9		
	0.9	0.04	<0.005	47.6		
	0.67	0.04	-0.01	47.2		

*After ref. 7.

Experimental error is about ±0.01 MHz; Θ_{shf} given with respect to a [110] axis.

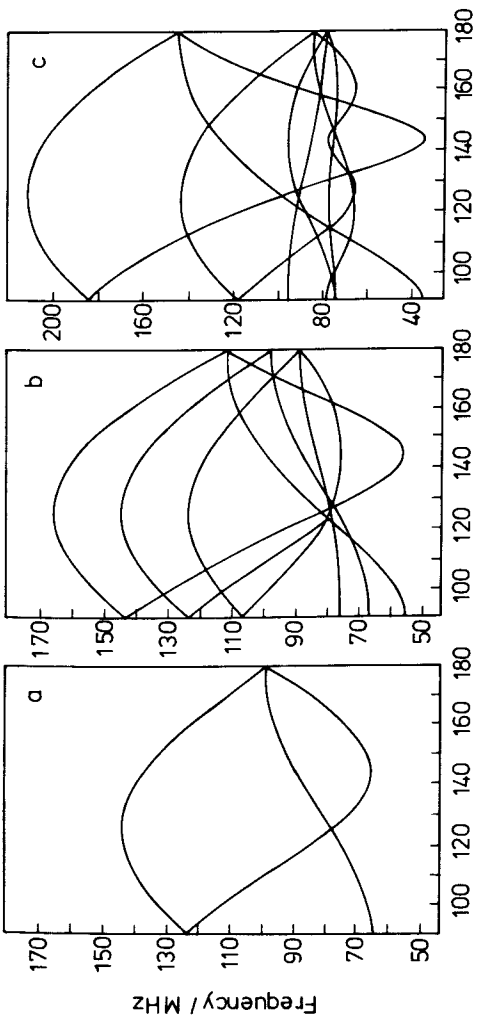

Figure 11 *Calculated ENDOR angular dependence of an assumed $AsAs_4$ antisite defect in GaAs due to four equivalent nearest ^{75}As neighbours for m_S = -1/2 and rotation of the crystal in a (110) plane from [110] = 90° to [100] = 180°.*
The simulation is for the following ligand hf and quadrupole constants (tensor axes //<111> directions)
(a) a/h = 198 MHz, b/h = 53 MHz, q/h = 0
(b) a/h = 198 MHz, b/h = 53 MHz, q/h = 3.5 MHz
(c) a/h = 198 MHz, b/h = 53 MHz, q/h = 11.1 MHz

quadrupole) interactions with several neighbour nuclei, which have exactly the same interactions both with respect to their interaction parameters and tensor orientations with respect to the magnetic field orientation B_0, e.g., if they are all precisely equivalent. Then an additional line splitting can occur, which can be quite confusing if not recognised as such (shf splitting of second order). The splitting pattern can be quite complicated. If there is only an isotropic shf interaction (or b << a) the the splitting between the ENDOR lines is of the order of $a^2/2g_e\beta_eB_0$. For small interaction constants it is hardly seen but it can show up clearly for large interactions (for a/h = 100 MHz, the splitting is of the order of 500 kHz).[15] In particular, if b and q are not small with respect to a, rather large splittings and a complicated pattern can occur. A recent example shows this in the ENDOR spectrum for the Ga-vacancy in GaP (Figure 12). For the particular orientation of B_0//<111> one would expect without this shf structure of second order only four ENDOR lines due to the four nearest ^{31}P neighbours, since for each m_s-value B_0 is parallel to the shf axis of one neighbour, the other three have the same angle with respect to B_0, thus yielding only two ENDOR lines. In the frequency range of Figure 12 there should be just four lines observed due to the four equivalent ^{31}P neighbours for $m_s = \pm 3/2$. There are, however, nine lines observed with large splittings of the order of several MHz. At first it was not clear whether the vacancy is distorted or not. The distortion could also give rise to splittings. DOUBLE-ENDOR experiments showed, however, that this splitting is due to the shf structure of second order. A full diagonalisation of the spin Hamiltonian for the case of four equivalent nuclei confirmed that the splitting is due to second order effects.[16]

In practice, another fact renders the ENDOR analysis rather difficult. If there are many lines due to one defect within a narrow frequency range, as is the case, e.g., for the atomic hydrogen centres on anion sites, then an analysis is only feasible by employing computer aided methods. Figure 13(a) shows the angular dependence of these centres. Another example is that of Ni^{3+} in GaP, where for each magnetic field orientation over 600 ENDOR lines were observed.[17] The angular pattern can also become complicated due to many centre orientations of low symmetry defects and due to the fact that the angular dependence must be described by a complete diagonalisation of the spin Hamiltonian. The result of this for the hydrogen centre is shown if Figure 13(b) using the shf and quadrupole constants of Table 1.

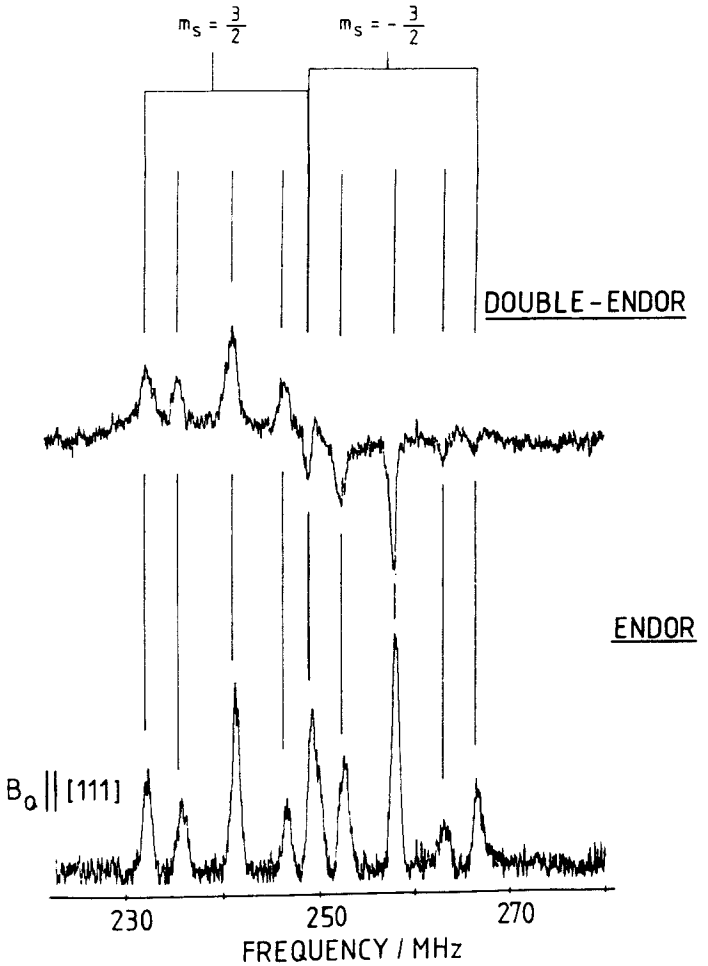

Figure 12 *(lower trace) ENDOR lines of ^{31}P nearest neighbours of the gallium vacancy (V_{Ga}) in GaP.B_0 approximately parallel to <111>; (upper trace) DOUBLE-ENDOR lines. (After ref. 10)*

Because of this, with conventional ENDOR spectrometers only comparatively simple problems could be solved. In complicated cases the angular dependence must be measured in small angular steps and due to a low signal-to-noise ratio, as is often observed, the experiments must be repeated many times. In recent years considerable

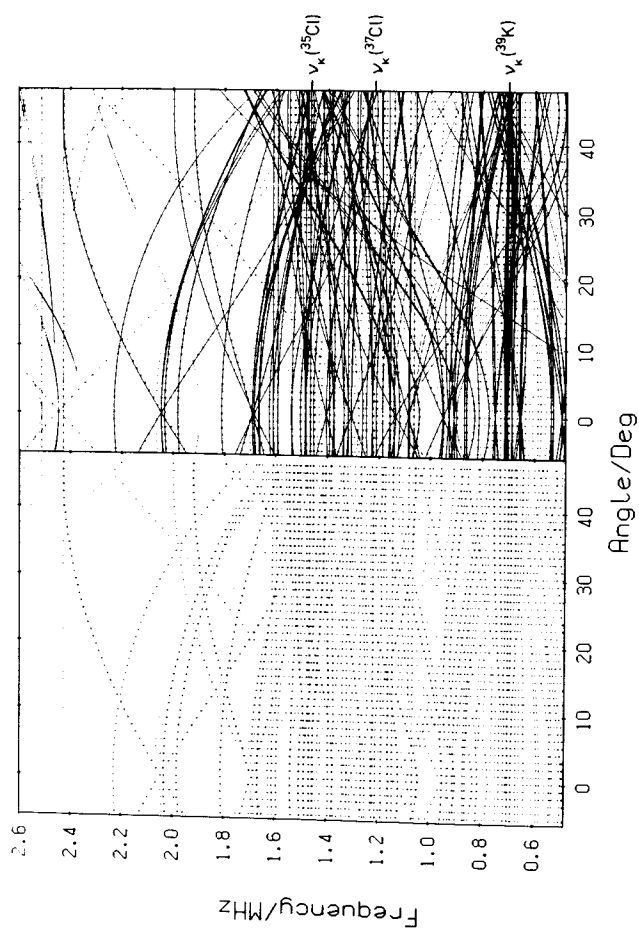

Figure 13 *Angular dependence of the ENDOR lines of atomic hydrogen centres on anion sites in KCl for rotation of the magnetic field in a (100) plane between <100> (0°) and <110> (45°). (left) Experimental results; (right) calculated angular dependence with the shf and quadrupole constants given in Table 3 and experimental data. (After ref. 10)*

progress has been made by setting up computer controlled ENDOR spectrometers and by using computers for the data processing and analysis of the spectra.

4.3 Experimental Aspects. - The possibility of observing a stationary ENDOR effect from solid state defects depends mainly on two essential parts of the spectrometer: (i) a suitable ENDOR cavity, which allows the generation of a strong enough rf amplitude B_2 without the quality factor Q of the cavity being affected too much, since the microwave amplitude B_1 must be high enough partially to saturate the ESR signal; (ii) a cryosystem, which allows variation of the sample temperature in a wide range, preferably between 1.5 K and room temperature. If the rf field is produced by a coil, in which rf current flows, one needs a TM-mode cavity.[18,19] A partic-

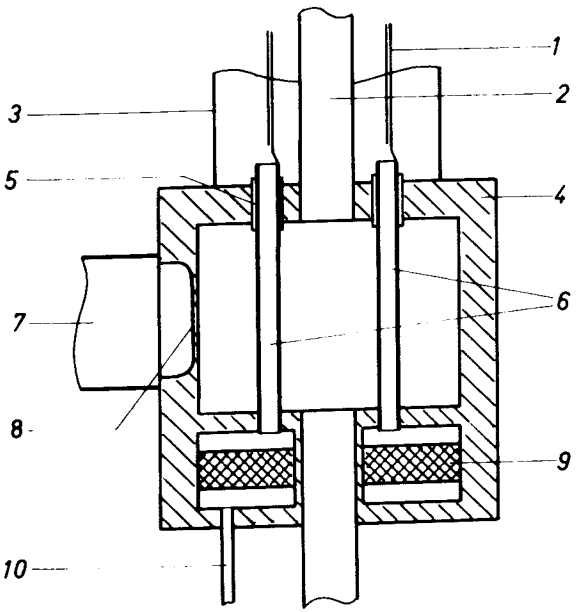

Figure 14 *ESR/ENDOR resonator for variable low temperature measurements from 3-300 K. The cylindrical resonator works in the TE_{011} mode. 1: rf connection; 2: tube to insert sample; 3: tube for helium exhaust gas; 4: resonator wall; 5: insulating rings (Teflon); 6: 4 silver tubes; 7: microwave guides; 8: iris; 9: heat exchanger; 10: liquid helium supply. (After ref. 21)*

ularly useful cavity construction is that of Figure 14, where the rf current flows through solid rods in a TE_{011} resonator.[20,21] The reason for the need to vary the sample temperature in a wide range is that, in order to observe the stationary ENDOR effect, the electron lattice relaxation rate $1/T_1$, the electron cross relaxation rate $1/T_x$ and the microwave transition rate for saturating the ESR transitions must all be of the same order of magnitude and they must be in certain relations with respect to each other. Because of the complex relaxation scheme in solids the optimum experimental conditions cannot be predicted. The best way is to be able to vary both microwave power and temperature and find experimentally the optimum conditions. Experience shows that often ENDOR measurements are possible only in a very narrow temperature range. The temperature must be neither too high nor too low, and this temperature range varies with the defect system. As a general rule, s-type electron ground states require higher temperatures (typically 30-70 K), p-type ground states (hole centres, acceptors in semiconductors) rather low temperatures. The availabilty of suitable cavity-cryostat combinations for solid state investigations is the most serious deficiency of commercial ENDOR spectrometers.

Since at low temperatures the nuclear spin lattice relaxation times are long, one cannot afford to use fast modulation of the rf fields. It was therefore first successful to build superheterodyne spectrometers, which were sensitive also for low modulation frequencies (20-1000 Hz). Since, however, the low noise microwave amplifiers has become available, its use to preamplify the signal before the microwave diode has proved to be approximately as sensitive as a superheterodyne setup with the advantage of being able to use the more simple and carefree homodyne spectrometers.[22]

The fact that in practical cases of interest many ENDOR lines appear and that the angular dependence of the ENDOR lines must be measured in small angular steps, which means continuous measurements for several weeks, called for computer aided techniques both for the experiment and for the analysis of the spectra. In the computer controlled ENDOR spectrometer the computer controls the following parameters: rf (NMR) frequencies, magnetic field, crystal orientation, sample temperature, and cavity matching. Thus, the angular dependence can be measured automatically, also as a function of temperature. A full angular dependence can take up to several weeks of continuous measurement. The ENDOR lines are stored in the computer and with specially developed software (see below) their positions can be determined automatically and a computer plot of the angular

dependence can be made. Figure 13(a) is such a plot.

The application of digital methods to the processing of the experimental data is summarised in Figure 15 for the example of

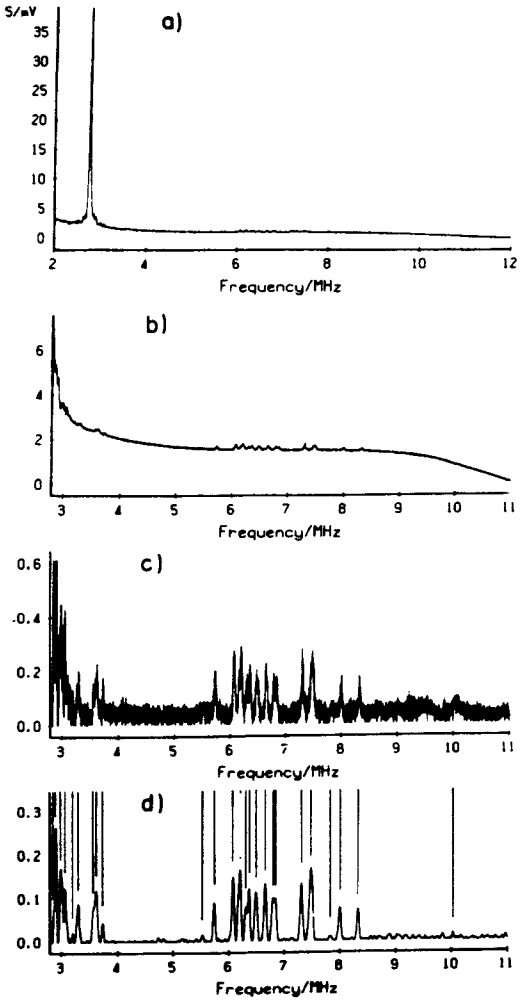

Figure 15 *Digital data processing for an ENDOR spectrum of interstitial Fe^0-centres in silicon. (a) spectrum as measured; (b) subtraction of the strong ENDOR signal at ν_n (^{29}Si) due to distant nuclei; (c) subtraction of a smooth background line; (d) digital filtering and application of the peak search algorithm. (After ref. 23)*

interstitial Fe^0 centres in Si.[23] Figure 15(a) shows the ENDOR lines of interest between 6 and 8 MHz, which are very weak compared to the 'distant ENDOR' due to the ^{29}Si nuclei with very low interaction and to a strong background signal. The latter and the distant ENDOR must be subtracted in order to deal better with the lines of interest. With a special algorithm the background is subtracted; it does not assume a particular form of the background. It 'eliminates' the sharp peaks from the rest, which then is subtracted from the total spectrum.[24] The resulting spectrum is that of Figure 15(c), which contains a number of ENDOR lines and, of course, noise. The signal-to-noise ratio of ENDOR spectra is usually not too good. The ENDOR effect in solid state defects is mostly below 1% of the ESR signal. Low defect concentration and the limited ENDOR effect are the major reasons for the poor signal-to-noise ratio. Here the use of digital filtering has proved to be very advantageous. The major concept is to smooth the spectra without disturbing the signals. Conventional RC-filters have a poor trade-off between noise reduction, signal distortion and speed of measurement. A simple digital method would be a running average algorithm, which replaces a data point by the average of the original data points and its unfiltered left and right neighbour points. This symmetric average over (2N + 1) data points produces the classic noise reduction of any averaging process of uncorrelated data. The idea can be improved by assigning different weights to the neighbouring data points.

$$f[K] = \sum_{i=-N}^{N} a[i].Y\,[K - i] \qquad (4.11)$$

where Y denotes the unfiltered and f the filtered data points. The weights a[i] describe the digital filter used. For a simple running average one has

$$a[i] = \frac{1}{(2N + 1)} \qquad (4.12)$$

If it is required that the filtering process conserves additive constants, linear slopes, and parabolic peaks, area, second and third moments and minimises noise under these constraints, it can be shown that the weight function

$$a[i] = \frac{3[(3N^2 + 3N - 1) - 5i^2}{[(2N - 1)(2N + 1)(2N + 3)]} \qquad (4.13)$$

is optimal for any line shape.[25] Such a filter is called a DISPO

filter (digital smoothing with polynomial coefficient).[26] Compared to an RC-filter it typically decreases the signal distortion by a factor of 20. For small signal distortion (1%) and equal scan speed it reduces the noise by an additional factor of 5 compared to the RC-filter.[27,28]

Figure 15(d) shows the application of such a filter to the spectrum of Figure 15(c). The line positions are determined by a special peak search algorithm in which the second derivative of the smoothed spectrum is calculated. A peak appears where this has a local minimum.[21] This is exact for symmetrical ENDOR lines of Gaussian of Lorentzian shape. The meaurement must make sure that the line shape remains symmetrical for this to be applied. Therefore, for this kind of ENDOR spectroscopy, the method of 'transient ENDOR' originally introduced by Feher[1] is not applicable, since there the line shapes are non-symmetrical.

When too many ENDOR lines overlap, the application of the peak search algorithm is not sufficient. An improvement can be effected by applying a deconvolution algorithm, which decomposes the spectra in an iterative process, since the exact shapes and widths of the single ENDOR lines are not known beforehand.

Figure 16(a) shows a section of a spectrum. After the application of the deconvolution procedure one obtains Figure 16(b). In Figures 17(a) and (b) the ENDOR angular dependences of $H^0_{s,a}$-centres in KCl with and without application of the deconvolution are compared. The advantages of this procedure are clearly seen in the section between 1.45 - 1.50 MHz and 1.20 - 1.25 MHz. The angular dependence can be followed much better and can be analysed. The analysis yields the anion vacancy as the site for the H^0 atom, the values of the shf and quadrupole interaction constants given in Table 1 being an example of typical ENDOR results and their precision. The spin Hamiltonian had to be diagonalised numerically.[10,14]

4.4 Dynamical Effects, Defect Reactions and Energy Levels studied by Endor. - By measuring the temperature dependence of ENDOR lines one can study dynamical properties of defects. An example is the influence of localised vibrations of atomic hydrogen centres in alkali halides on the ENDOR line positions,[9,29,30] as well as the influence of the structural phase transition in $RbCdF_3$ on Mn^{2+} defects.[31,32] Defect reactions can also be studied by ENDOR. Recently the conversion of F centres in KCl doped with F^- to $F_H(F^-)$ centres was studied. The ESR spectrum of the new $F_H(F^-)$ centre cannot be distinguished from that of the F centre, but its ENDOR spec-

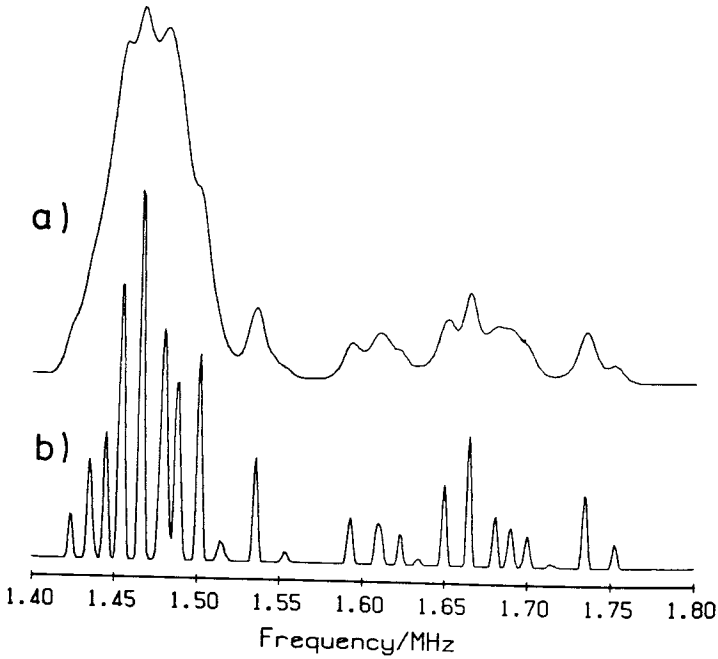

Figure 16 *Deconvolution of spectra to enhance the resolution of ENDOR. (a) spectrum as measured; (b) after application of the deconvolution algorithm. (After ref. 21)*

trum is very different. The structure of the $F_H(F^-)$ centre could be established.[33] Also, the aggregation of interstitial oxygen in Si to form the so called 'thermal donors' showed up in ENDOR as a function of the annealing time at 450 °C.[36,37]

It is often important not only to know the defect structure but also its energy level. In semiconductors this can be achieved in samples where the Fermi level is below the level in question, which is then not occupied by electrons and no ESR/ENDOR can be measured. However, upon illumination with light of variable energy it can be occupied from the valence band and ESR/ENDOR measurements under the illumination of the correct photon energy are possible. From the onset of these photo-ESR/ENDOR experiments the level position can be determined. A recent example is that of S^+, Se^+ and $(S\text{-}S)^+$, $(Se\text{-}Se)^+$ defects in Si.[36,37]

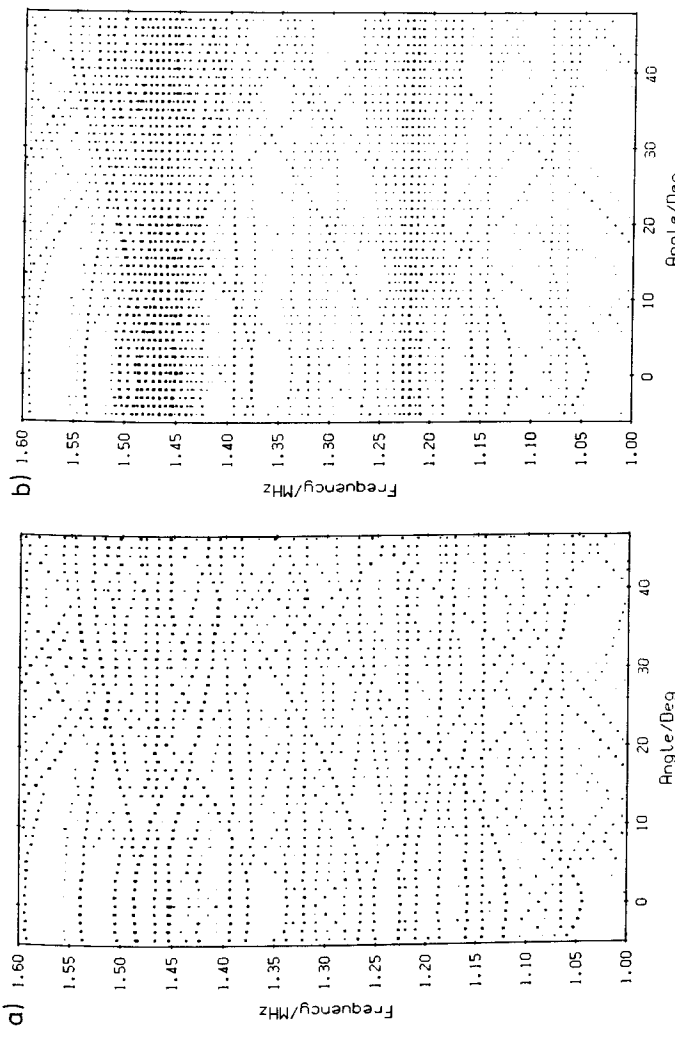

Figure 17 *(a) Section of the ENDOR angular dependence of Figure 13 (atomic hydrogen on anion sites in KCl) obtained after digital filtering of the experimental lines and application of the peak search algorithm; (b) the same section after the additional application of the deconvolution algorithm. (After ref. 21)*

5. Advanced ENDOR Methods

5.1 ENDOR-induced ESR. - Overlapping ESR spectra of different defects cause overlapping ENDOR spectra. It can be very difficult if not impossible to analyse their angular dependence, especially if many ENDOR lines occur in a narrow frequency range. Furthermore, there may be weaker ESR spectra buried under stronger ones having observable ENDOR lines, which can be analysed, but the ESR spectrum cannot be measured. The two types of F centres possible in BaFCl for example are produced simultaneously. Their ESR spectra strongly overlap (see Figure 18). In such a case one can measure a kind of excitation spectrum of a particular ENDOR line belonging to one defect, which gives an image of the corresponding ESR spectrum belonging to the same defect (ENDOR-induced ESR spectrum). This can be seen from Figure 6. The ENDOR transitions can be measured by setting B_0 to any of the four shf ESR transitions for m_I = 3/2, 1/2, -1/2 and -3/2, thus the ENDOR line intensity measured should follow the ESR line pattern in the middle of Figure 6. According to equation (4.6), however, the frequency of an ENDOR line depends on ν_n and therefore on B_0. Because of this one must 'correct' the ENDOR frequency for the variation of B_0 when varying B_0 through the ESR spectrum. This can easily be done with the computer controlled spectrometer or other ways provided the corresponding nuclear g_I factor is known. In measuring the ENDOR-induced ESR spectrum one monitors the ENDOR line intensity of a particular ENDOR line, while varying the magnetic field through the ESR spectrum and correcting the frequency position according to equation (4.6). The resulting spectrum is an image of the (integrated) ESR spectrum of that defect to which the ENDOR line (nucleus) belongs. In this way the ESR spectra of different defects can be separated.

Figure 18 shows this for the two F centres in BaFCl. The two ENDOR-induced ESR spectra were measured using ^{19}F ENDOR lines of both centres. If S = 1/2 and if no quadrupole interaction is experienced by the nucleus, the ENDOR-induced ESR spectrum corresponds to the true ESR line shape, if the cross relaxation does not depend on m_I and is not the dominating electron spin relaxation process. This was observed in several cases.[38]

The line shape of the ENDOR-induced ESR spectrum is not necessarily identical with that of the ESR spectrum. To discuss this let us consider Figure 19, where the level scheme for the simplified case S = 1/2, I = 3/2 and W_{shf} and $W_q \neq 0$ is assumed. If one uses the ENDOR transitions between levels A and B for the ENDOR-induced ESR experiment, only the two ESR transitions between levels B and C

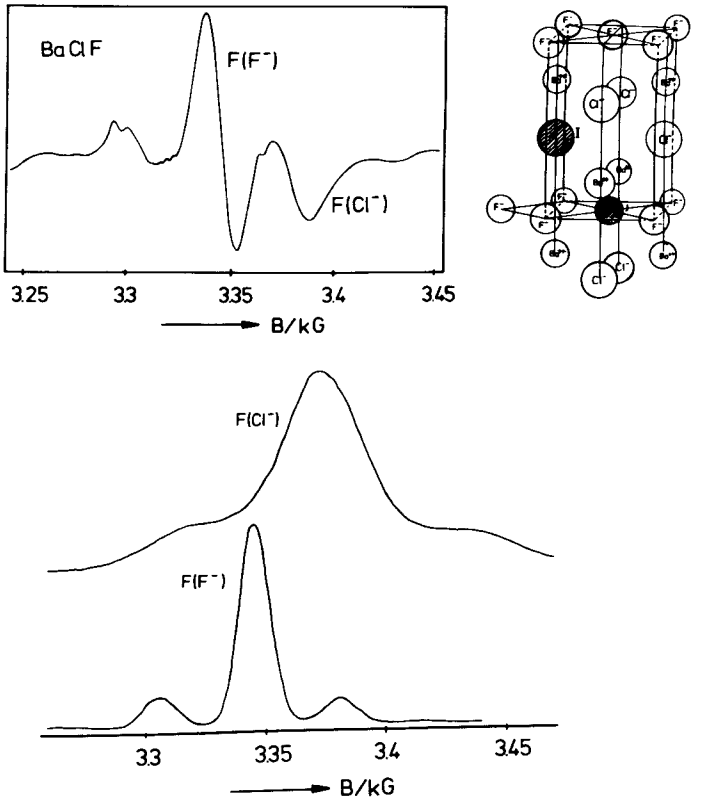

Figure 18 *Model of two F-centres in BaFCl [F(Cl⁻) and F(F⁻) centres], their superimposed ESR spectra (derivative) and the ENDOR-induced ESR spectra of both centres measured using a ^{19}F ENDOR line of each centre. (After ref. 44)*

and A and D are affected. For instance, the partially saturated ESR transition D-A is desaturated by the NMR transition A-B. Similarly, the ESR transition C-B is experiencing a population change due to the NMR transition A-B. The other two possible ENDOR transitions are not affected. Thus, using any of the three quadrupole ENDOR lines, only for two ESR transitions, the m_I states of which are connected to the ENDOR transition, the double resonance condition is fulfilled. They can only be seen as ENDOR-induced ESR spectra if the following holds:

(i) only the simple type of cross relaxation process (m_s, m_I) ($m_s = -1$, $m_I = \pm 1$) occurs;

(ii) no significant relaxation takes place between different m_I states within a given m_s state.

An example of this is shown in Figure 20, where the two line ENDOR-induced ESR spectrum was measured locking the ENDOR frequencies successively to the three ENDOR lines of the Ba^{2+} quadrupole triplet of $F(Cl^-)$ centres in BaFCl. The assumption seems to hold quite well,

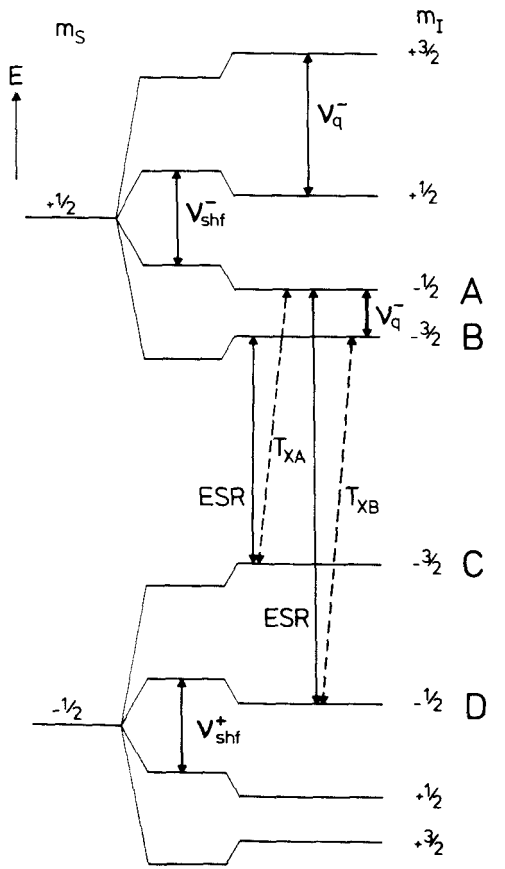

Figure 19 *Schematic representation of the energy levels for the system S = 1/2, I = 3/2 with shf and quadrupole interactions. The arrows denote ESR/ENDOR and cross relaxation transitions.*

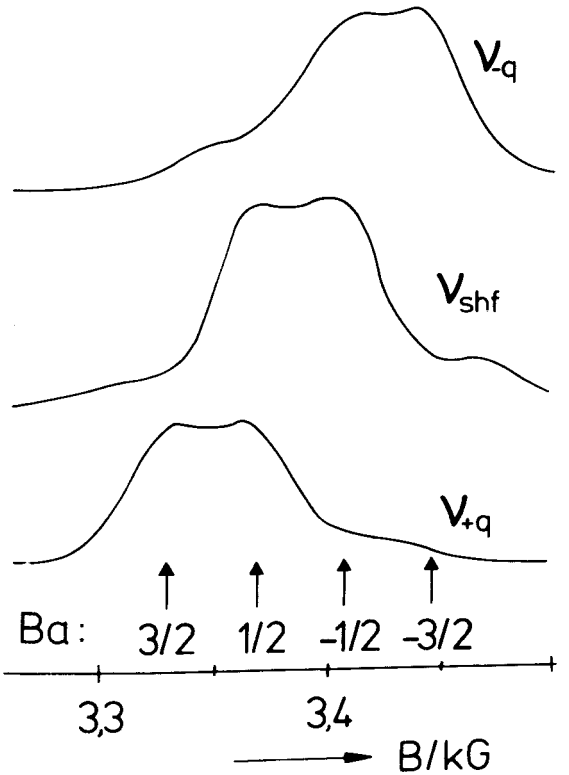

Figure 20 *ENDOR-induced ESR spectra of F(Cl⁻) centres in BaFCl using the ^{137}Ba quadrupole triplet ENDOR lines ν_q^-, ν_{shf} and ν_q^+. (After ref. 38)*

although not perfectly, as the small intensity of the two further lines in the ENDOR-induced ESR spectra indicates.

The true line shape of the full ESR spectrum is observed if there is no quadrupole interaction and if the relaxation times T_x do not depend on the nuclear spin states. Neglecting isotope mixture, the arguments given above for one neighbour also apply for a nucleus out of many neighbours, the ENDOR line of which is taken for the ENDOR-induced ESR measurement.

The line shape observed for the ENDOR-induced ESR line is discussed in detail in refs. 38 and 39. As a general 'rule' it can be said that the line shape is almost the true ESR line if an ENDOR line of a nucleus with a very small interaction (i.e., distant shell

neighbour) is taken for the experiment. The selection of spin states allows the determination of the relative signs of W_q and W_{shf}. From Figure 20 it can be concluded that both W_{shf} and W_q have the same sign as in the case of Figure 19.

There are certain complications if different isotopes are present. Suppose there is only one nucleus with different isotopes, e.g., ^{37}Cl and ^{35}Cl, and a shf-ENDOR line of one isotope is used for ENDOR-induced ESR, then the line shape is not the true ESR line shape. In order to obtain this, one has to add the ENDOR-induced ESR spectra due to all the corresponding ENDOR lines of the different isotopes. The intensity ratio of the different ENDOR-induced ESR spectra should correspond to the abundances of the different isotopes. If this is not so, then the cross relaxation rates are different for the isotopes. To obtain the true line shape in this case would require a knowledge of this latter effect in order to correct the superposition of the isotope ENDOR-induced ESR spectra.

If there are more nuclei of a type with different isotopes, similar arguments apply. One has to add the isotope ENDOR-induced ESR spectra of the nuclei used for the measurement. More serious complications arise if several strongly coupled nuclei show effects of second order shf splitting.[15,16] One then has to work in the total spin representation and the understanding of the ENDOR-induced ESR spectra is less straightforward. A detailed discussion of this problem would be beyond the scope of this Chapter. Results obtained for F^+ centres in Na-β-alumina where two Al nuclei are strongly coupled are described in ref. 40.

For systems with $S > 1/2$ there is usually a fine structure interaction splitting of the electron Zeeman levels. In this case with ENDOR-induced ESR one selects spin states in an analogous way to the selection of m_I states due to the quadrupole interaction discussed above. One measures only some of the possible ESR transitions. This is demonstrated for Fe^{3+} centres in $KMgF_3$, which were produced by X-irradiation of $KMgF_3$ doped with Fe^{2+}. In Figure 21(a) the integrated ESR spectrum of the five ESR transitions is reproduced with partly resolved shf structure with six nearest ^{19}F neighbours. Figure 21(b) shows the ENDOR-induced ESR spectrum measured with a ^{19}F ENDOR line at 42.5 MHz displaying two of the five Fe^{3+} ESR transitions, while Figure 21(c) shows the ENDOR-induced ESR spectrum measured with a ^{19}F ENDOR line at 21.0 MHz. Clearly, another ESR spectrum appears. It was buried under the Fe^{3+} spectrum beyond recognition and turned out to be due to simultaneously produced F centres.[41] A detailed analysis also allows the determination of the relative signs of

quadrupole interaction constants, shf interaction constants and fine structure constants.[38,39]

5.2 DOUBLE-ENDOR. - Although with ENDOR-induced ESR experiments

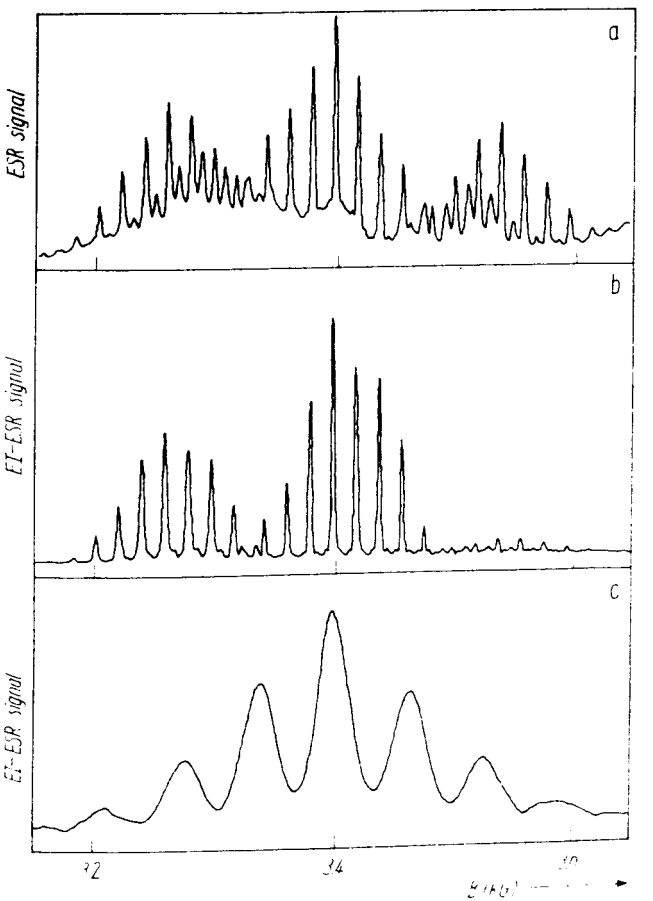

Figure 21 *ESR and ENDOR-induced ESR spectra of X-irradiated $KMgF_3$ doped with Fe^{3+}. (a) integrated ESR spectrum after X-irradiation at room temperature. B_0//<100>; (b) ENDOR-induced ESR spectrum for the ^{19}F-ENDOR lines at 42.5 MHz - the spectrum is due to Fe^{3+}; (c) ENDOR-induced ESR spectrum for the ^{19}F-ENDOR lines at 21.0 MHz - the spectrum is due to F-centres. (After ref. 45)*

each ENDOR line can be 'labelled' to a particular defect, in the case of the simultaneous presence of several defects this can be a tedious task, especially if one has to follow a complicated angular dependence. Therefore, a method is required with which the ENDOR spectra of different defects can be measured separately, this can be done by measuring a triple resonance, in which two NMR frequencies are applied simultaneously together with the microwaves.

In an ENDOR experiment the rf-induced NMR transitions between the nuclear Zeeman levels of a neighbour nucleus coupled to the unpaired electron by a shf interaction change somewhat the polarisation of the electron spin in the partially saturated situation. This coupling between neighbour nucleus and unpaired electron is indicated schematically by a 'spring' in Figure 22. If simultaneously a second

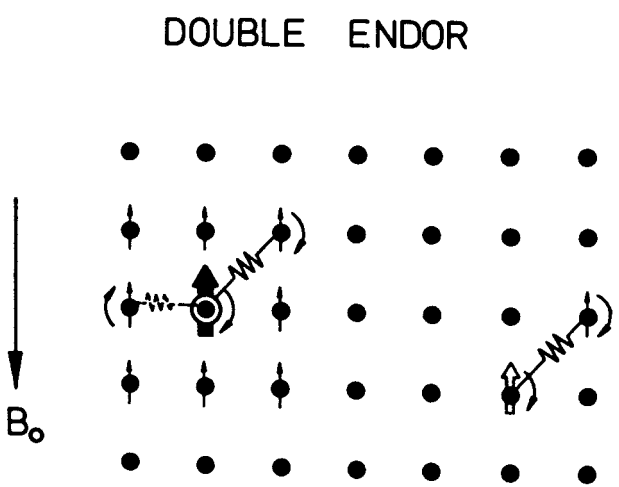

Figure 22 *Schematic representation of ENDOR and DOUBLE-ENDOR*

NMR transition is induced with a second rf frequency at another nucleus coupled to the same unpaired electron, then the induced change in the electron spin polarisation is different from what it would be if the first NMR transition did not occur simultaneously. Thus, the polarisation change due to the second NMR transition is dependent on the occurrence of the first NMR transition. The total electron desaturation (ENDOR effect) is a function of the product of the effects of the two NMR transitions. Thus, when modulating the two NMR transitions with different frequencies, using double lock-in

techniques, one can induce one particular ENDOR transition of a particular neighbour nucleus and monitor the change in the ENDOR signal height as a function of the simultaneous second ENDOR transition. One observes changes in the NMR line intensity as a function of the second frequency swept rf source. A change is observed when a second ENDOR transition is induced at a nucleus that is also coupled to the same electron, but not if the nucleus belongs to a different centre. The ESR of this different centre may also be saturated if the ESR spectra of the different centres overlap. Therefore, this triple resonance experiment can be used to separate the ENDOR spectra of different defects if their ESR spectra overlap. Such a separation may well otherwise be impossible if the centres have many ENDOR lines with complicated angular dependencies. However, the method functions well only if the neighbours have a high

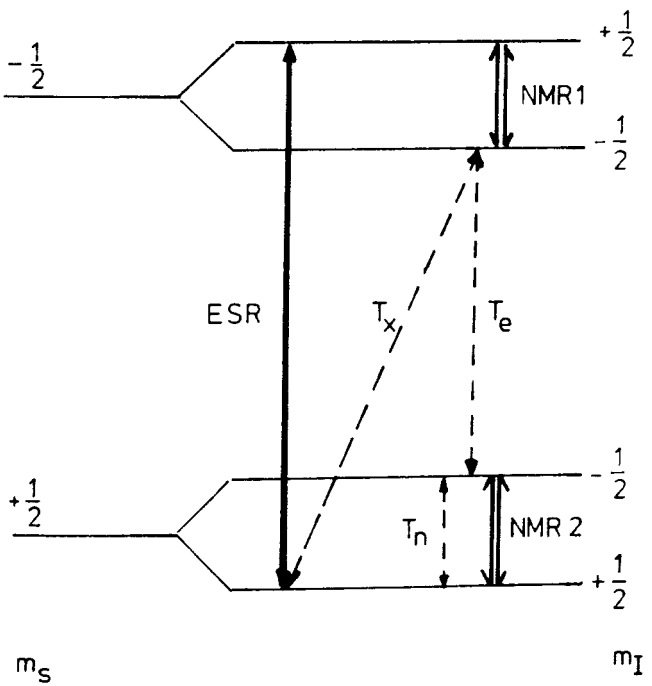

Figure 23 *Level scheme to explain the special triple resonance experiments (DOUBLE-ENDOR)*

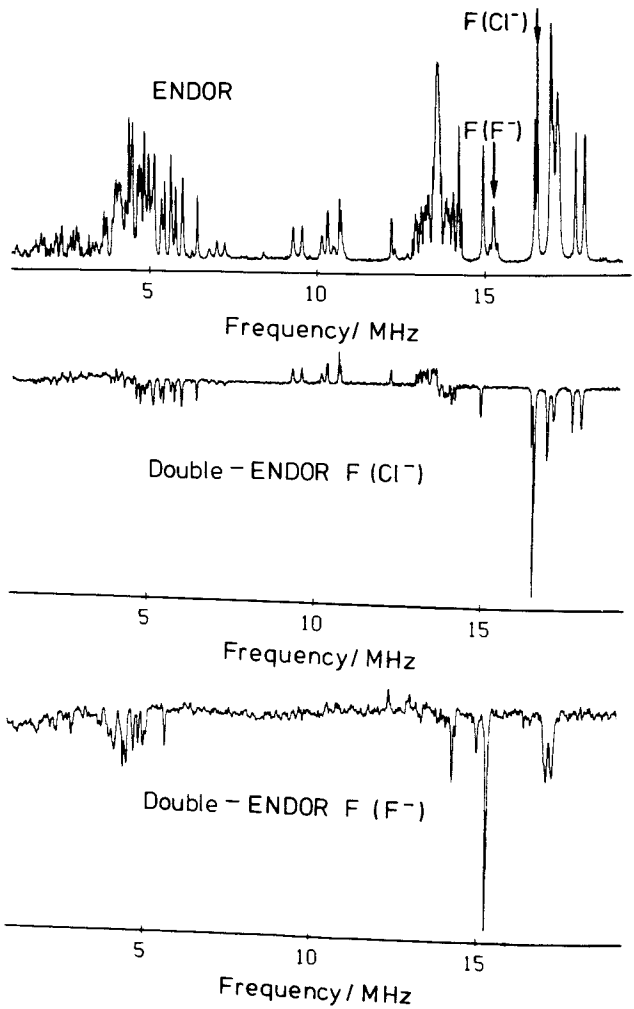

Figure 24 *(a) Part of the ENDOR spectrum of $F(Cl^-)$ and $F(F^-)$ centres simultaneously present in BaFCl; (b) DOUBLE-ENDOR spectrum obtained from setting one frequency to an ENDOR line of $F(Cl^-)$ centres (see arrow in Figure 24) and sweeping the second rf frequency; (c) DOUBLE-ENDOR spectrum obtained from setting on rf frequency to an $F(F^-)$-ENDOR line (see arrow in Figure 24). (After ref. 44)*

abundance of magnetic nuclei. In Si, where only 4.7% of the nuclei are magnetic (^{29}Si), the probability of having simultaneously two magnetic nuclei as defect neighbours is too low to permit DOUBLE-ENDOR experiments.

The simplest experiment, the so called 'special triple resonance' (special DOUBLE-ENDOR) is schematically shown in Figure 23 for the simple case of S = 1/2, I = 1/2. If stationary ENDOR is measured for the transition 'NMR1' between $m_S = -1/2$, $m_I = 1/2$ and $-1/2$, then the signal height is determined by the ESR transition probability (that is by B_I^2), the NMR1 transition probability [that is B_{rf}^2 (NMR1)] and the cross relaxation time T_x. It is assumed (and a condition for the experiment), that $T_x > T_e$, the electron spin lattice relaxation time, due to the comparatively long nuclear spin lattice relaxation time T_n. If then a second rf frequency is applied between the levels $m_S = 1/2$, $m_I = 1/2$ and $-1/2$ (NMR2) then T_n is effectively shortened by this transition and therefore T_x is also shortened, which results in an enhancement of the monitored ENDOR signal at the frequency NMR1. In the experiment one irradiates with the fixed ENDOR frequency NMR1, monitors the ENDOR line intensity of the line at NMR1, while sweeping the second rf frequency. When the transition NMR2 is induced the ENDOR line intensity NMR1 increases. The increase is the DOUBLE-ENDOR signal and is detected with a double lock-in technique.

In the stationary DOUBLE-ENDOR spectrum positive and negative signals are observed.[42,43] Negative signals occur if the second NMR frequency is induced between nuclear states belonging to the same m_S quantum number. Figure 24(c) shows the DOUBLE-ENDOR spectrum for the two F centres in BaFCl. In Figure 24(a) the ENDOR lines of both F centres are superimposed; a full analysis was not possible. In Figure 24(b) the fixed ENDOR frequency NMR1 was set to one ENDOR line belonging to $F(Cl^-)$ centres and NMR2 was swept between 1 and 9 MHz and the DOUBLE-ENDOR effect was recorded. In Figure 24(c) the analogous experiment was carried out for a $F(F^-)$ ENDOR line. Both DOUBLE-ENDOR spectra show only lines due to the $F(Cl^-)$ of $F(F^-)$ centres alone. Especially around 5 MHz both centres have many ENDOR lines, which otherwise could not have been separated.[44]

Figure 12(a) shows as another example the DOUBLE-ENDOR spectrum measured for the Ga-vacancy in GaP for $B_0 // \langle 111 \rangle$. Comparison with Figure 12(b) demonstrates that all the lines measured in single ENDOR also appear in DOUBLE-ENDOR. This proves that all ENDOR lines belong indeed to one defect and that the vacancy is not distorted with the consequence that the ENDOR spectrum might be a superposition of several vacancy configurations. The occurrence of so many

ENDOR lines, at first unexpected for a simple tetrahedral surrounding of four equivalent ^{31}P neighbours, is indeed due to a large and hitherto undescribed effect of shf structure of second order.[16]

DOUBLE-ENDOR is also very important for analysing low symmetry defects. The defects are distributed over several orientations in the crystal. The ESR and ENDOR spectra of these orientations overlap. In a sense each defect orientation is equivalent to a new defect species. With DOUBLE-ENDOR the spectra of one particular defect orientation can be measured separately, which greatly facilitates the analysis or makes it all possible. In a recent investigation of $\bar{O}$ centres in α-Al_2O_3, which has very low symmetry (that is 'no' symmetry), a definite assignment of the quadrupole ENDOR lines to their corresponding 'hf' ENDOR lines was only possible after one particular centre orientation could be measured separately.[45]

6. Optically detected ENDOR

Recently ENDOR could successfully be measured also by optical detection using the optical absorption of defects in III-V semiconductors and in ionic crystals. The optical detection of ESR is based on the detection of microwave-induced changes of the magnetic circular dichroism (MCD) of the optical absorption as was first shown for F centres in alkali halides.[46] The MCD is proportional to the spin polarisation of the ground state Zeeman levels. For a Kramer's doublet with S = 1/2 it is given by

$$\mathrm{MCD} = 1/2\alpha_0 \cdot \frac{\sigma^+ - \sigma^-}{\sigma^+ + \sigma^-} \cdot \frac{n_- - n_+}{n_- + n_+} \qquad (6.1)$$

where α_0 is the absorption constant of the unpolarised light, σ^+ and σ^- are the cross sections for left and right polarised light, respectively, and n_- and n_+ are the occupation numbers for the $m_s = \pm 1/2$ states. The occupation difference or spin polarisation can be decreased by a microwave transition, provided the microwave transition rate is of the order of or larger than the spin lattice relaxation rate $1/T_1$. The ESR transition thus results in a decrease of the MCD, which is monitored.[46]

Figure 25 shows the level scheme for the case of S = 1/2, a central nucleus with $I_c = 3/2$ and one ligand nucleus with I = 3/2 (e.g., a simplified model for the $EL2^+$ defect in GaAs). In the experiment one sets the magnetic field onto a particular position of the ODESR line, e.g., into the flank. ESR transitions must obey the selection rule $\Delta m_I = 0$, $\Delta m_s = \pm 1$. Thus, when measuring the ESR in one of the four lines of the $I_c = 3/2$ system, then at most a quarter of the all

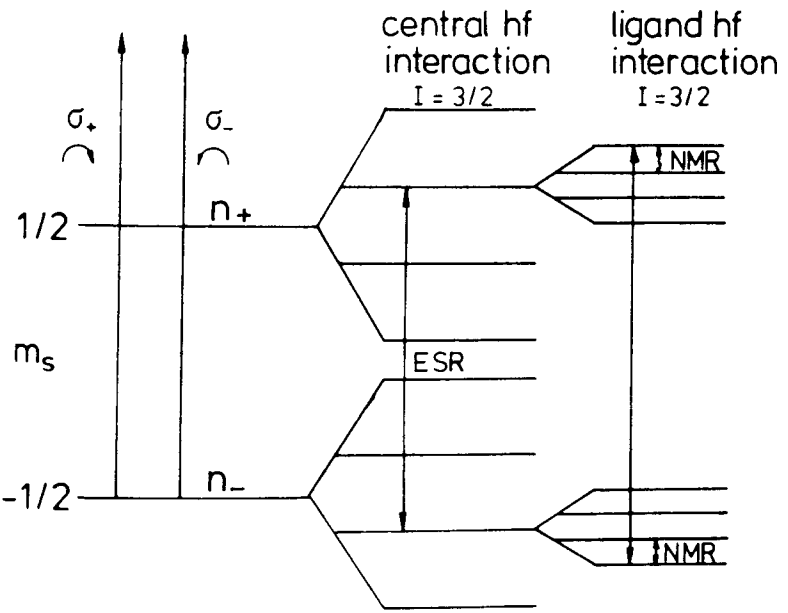

Figure 25 *Level scheme to illustrate the detection of ENDOR via a rf and microwave-induced decrease of the MCD of the optical absorption*

spin packets can be involved, only one quarter of the MCD can be decreased when saturating the transition. However, if each of the lines is inhomogeneously broadened by further shf interactions, then only a fraction of the decrease should occur, since $\Delta m_{I,a} = 0$ must be obeyed for the ligand I_a. Thus, upon inducing NMR transitions between the nuclear Zeeman levels, one can include more $m_{I,a}$ substates into the ESR pumping cycle and thus increase the effect of decreasing the MCD. Therefore, the ENDOR transitions are detected as a further increase of the ODESR.

Figure 26 shows a section of the ODENDOR lines due to the nearest ^{75}As neighbours of the $EL2^+$ defect in an as-grown undoped GaAs crystal.[6,47,48] The ENDOR lines are as sharp and numerous as in conventional ENDOR. From their angular dependence the structure model of the EL2 defects could be derived.

A similar study was recently made for Pb^+ centres in CaF_2, SrF_2 and BaF_2, in which the structure was shown to be a Pb^+ on cation sites next to an F^- vacancy along <111>. The ^{19}F ENDOR lines measured in the MCD and their angular dependence clearly showed the

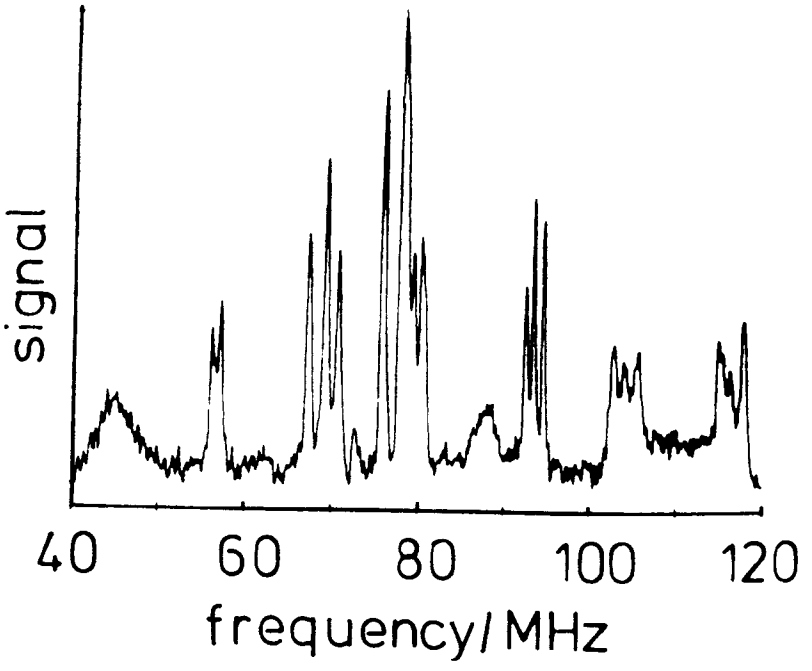

Figure 26 *Section of the ODENDOR spectrum of the $EL2^+$ defects in s.i. 'as grown' GaAs. T = 1.5 K, with B_0 in a (110) plane. The lines are due to five ^{75}As neighbours od the $AsGa^+$, which form the core of the $EL2^+$ defect. (After ref. 6)*

symmetry of the defect and its atomistic structure.[49,50] The signal-to-noise ratio of the ENDOR lines was very good, as it also is for $EL2^+$.

There are several advantages for the optical detection of ENDOR with the MCD technique. The sensitivity is several orders of magnitude higher than in conventional ENDOR. In particular for the case of $EL2^+$ defects in semi-insulating GaAs, the ENDOR signal intensity is approximately 10^4 times higher than expected from simple spin statistics. This is not yet understood. Furthermore, the method is very selective, since only one single defect can be measured as long as its optical absorption does not fully overlap that of another defect. This was recently successfully used for $F_H(OH^-)$ centres in KBr, which occur in a bistable configuration at very low temperature and the optical absorption bands of which differ only slightly on

the high and low energy side.[51] A further advantage is the possibility of correlating ENDOR spectra with optical absorption bands via a sort of excitation spectroscopy of the ODENDOR lines ('tagging').[47,52] Finally, it opens up the possibility of performing spatially resolved ESR and ENDOR experiments, which is of high actual interest in current semiconductor research for characterising semiconductor wafers. As a first example the distribution of the two charge states of the EL2 defects, $EL2^+$ and $EL2^0$, were investigated across a semi-insulating GaAs wafer.[53]

Only a very few experiments were performed where ENDOR was observed in luminescence except for triplet states in organic systems.[54] In ionic crystals it was Tm^+ in CaF^2,[55] a rare earth defect. A few observations were recorded in semiconductors using the donor - acceptor recombination luminescence. There have been observations in amorphous Si[56,57] and in ZnSe,ZnSe.[58] The ENDOR lines were observed as an emission increase upon inducing NMR transmissions by a rf applied in a small loop attached to the sample. In ZnSe, for example, two lines due to ^{67}Zn and ^{77}Se were seen centred at the frequencies of the free nuclei. The emission enhancement effect was of the order of 1%. The ENDOR lines were broad, about an order of magnitude broader than in conventional ENDOR. No angular dependence was reported.[58] Using time resolved techniques the ENDOR of ^{115}In in ZnO could be observed.[59]

The observation of ENDOR via emission has a principal disadvantage. If the lifetime of an excited state giving rise to the emission is 1 s or shorter, then the homogeneous ENDOR linewidth is 1 MHz or more. Thus, one loses all the detailed information required for the structure determination. Furthermore, to be able to shift populations between nuclear Zeeman levels within the radiative lifetime one needs very high NMR probabilities requiring rf field strengths of 10 mT or more, which at low temperatures cause quite a technical problem.

7. Conclusions

ENDOR spectroscopy is a powerful tool for the investigation of defects in solids. The availability of modern experimental techniques including the application of computer aided methods makes it possible to tackle difficult problems of interest in materials science. The development of these methods is by no means complete. In particular, it is conceivable that the use of methods like expert systems in computer science may help to analyse difficult spectra. The optical detection of ENDOR opens up quite a new range of applic-

ations and should be developed further. An extension into further infrared would open up investigations in Si and the use of micro-optical techniques could improve spatial resolution and perhaps be applied to thin layers. The ENDOR detection via emission has not yet really been explored in inorganic systems. Much remains to be done.

References

1 G. Feher, *Phys.Rev.*, 1959, **114**, 1219, 1249.
2 A. Schweiger, in 'Electron Spin Resonance,' ed. M.C.R. Symons (Specialist Periodical Reports), The Royal Society of Chemistry, London, 1987, Vol. 10B, p. 138.
3 A. Abragam and B. Bleaney, 'Electron Paramagnetic Resonance of Transition Ions,' Clarendon Press, Oxford, 1970.
4 C.P. Slichter, 'Principles of Magnetic Resonance,' Harper & Row, 1963.
5 G.E. Pake and T.L. Estle, 'The Physical Principles of Electron Paramagnetic Resonance,' W.A. Benjamin, 2nd Edition, 1973.
6 B.K. Meyer, D.M. Hofmann, J.R. Niklas, and J.-M. Spaeth, *Phys.Rev. B*, 1987, **36**, 1332.
7 S. Greulich-Weber, J.R. Niklas, and J.-M. Spaeth, *J.Phys. C*, 1984, **17**, L911.
8 H.G. Grimmeiss, E. Janzen, H. Hennen, O. Schirmer, J. Schneider, R. Wörner, E. Holm, E. Sirtl, and P. Wagner, *Phys.Rev. B*, 1981, **24**, 4571.
9 J.-M. Spaeth, 'Atomic hydrogen as a model defect in alkali halides,' in 'Defects in Insulating Crystals,' ed. V.M. Tuchkevich and K.K. Shvarts, Springer, Berlin, Heidelberg and New York, 1981, p. 232.
10 G. Heder, J.R. Niklas, and J.-M. Spaeth, *Phys.Stat.Solid. (b)*, 1980, **100**, 567.
11 H. Seidel, *Z.Physik.*, 1961, **165**, 210, 239.
12 J.R. Niklas and J.-M. Spaeth, *Solid State Commun.*, 1983, **46**, 121.
13 F. Beeler, M. Scheffler, O. Jepsen, and O. Gunnarson, *Mater.Res.Soc.Symp. Proc.*, 1985, **46**, 117.
14 G. Heder, Dissertation, Paderborn, 1979.
15 T.T. Feuchtwang, *Phys.Rev.*, 1962, **126**, 1628.
16 J.Hage, J.R. Niklas, and J.-M. Spaeth, *Mater.Sci.Forum*, 1986, **10–12**, 259.
17 Y. Ueda, J.R. Niklas, J.-M. Spaeth, U. Kaufmann, and J. Schneider, *Solid State Commun.*, 1983, **46**, 127
18 K. Möbius and R. Biehl, in 'Multiple Electron Resonance Spectroscopy,' ed. M.N. Dorio and J.H. Freed, Plenum, New York, 1979.
19 C.P. Poole, jun., 'Electron Spin Resonance,' Wiley, New York, 1973.
20 H. Seidel, *Z.Angew.Phys.*, 1962, **14**, 21.
21 J.R. Niklas, Habilitationsschrift, Paderborn, 1983.
22 Ch. Hoentzsch, J.R. Niklas, and J.-M. Spaeth, *Rev.Sci.Instrum.*, 1978, **49**, 1100.
23 S. Greulich-Weber, J.R. Niklas, E. Weber, and J.-M. Spaeth, *Phys.Rev. B*, 1984, **30**, 6292.
24 J.R. Niklas, Habilitationsschrift, Paderborn, 1983.
25 M.U.A. Bromba and H. Ziegler, *Anal.Chem.*, 1979. **51**, 1760.
26 H. Ziegler, *Appl.Spectrosc.*, 1981, **35**, 88.
27 M.U.A. Bromba and H. Ziegler, *Anal.Chem.*, 1983, **55**, 648.
28 M.U.A. Bromba and H. Ziegler, *Anal.Chem.*, 1984, **56**, 2052.
29 Ch. Hoentzsch and J.-M. Spaeth, *Phys.Stat.Solid. (b)*, 1979, **94**, 479.
30 P. Studzinski, J.R. Niklas, and J.-M. Spaeth, *Phys.Stat.Solid. (b)*, 1980, **101**, 673.
31 P. Studzinski and J.-M. Spaeth, *Radiat.Effects*, 1983, **73**, 207.
32 P. Studzinski and J.-M. Spaeth, *J.Phys. C*, 1986, **18**, 6441.

33 H. Söthe, P. Studzinski, and J.-M. Spaeth, *Phys.Stat.Solid. (b)*, 1985, **130**, 339.
34 P. Wagner, C. Holm, E. Sirtl, R. Oeder, and W. Zulehner, in 'Festkorperprobleme: Advances in Solid State Physics,' ed. P. Grosse, Vieweg, Braunschweig, Vol. 24, 1984, p. 191.
35 J. Michel, J.R. Niklas, J.-M. Spaeth, and C. Weinert, *Phys.Rev.Lett.*, 1986, **57**, 611.
36 S. Greulich-Weber, Dissertation, Paderborn, 1987.
37 S. Greulich-Weber, J.R. Niklas, and J.-M. Spaeth, to be published.
38 J.-M. Spaeth and J.R. Niklas, in 'Recent Developments in Condensed Matter Physics 1,' ed. J.T. Devreese, Plenum, New York, 1981, p. 393.
39 J.R. Niklas and J.-M. Spaeth, *Phys.Stat.Solid. (b)*, 1980, **101**, 221.
40 R.C. Barklie, J.R. Niklas, and J.-M. Spaeth, *J.Phys. C*, 1980, **13**, 1745, 1757.
41 R.C. DuVarney, J.R. Niklas, and J.-M. Spaeth, *Phys.Stat.Solid. (b)*, 1980, **97**, 135.
42 B. Biehl, M. Plato, and K. Mobius, *J.Chem.Phys.*, 1975, **63**, 3515.
43 N.S. Dalal and C.A. McDowell, *Chem.Phys.Lett.*, 1970, **6**, 617.
44 J.R. Niklas, R.U. Bauer, and J.-M. Spaeth, *Phys.Stat.Solid. (b)*, 1983, **119**, 171.
45 R.C. DuVarney, J.R. Niklas, and J.-M. Spaeth, *Phys.Stat.Solid. (b)*, 1985, **128**, 673.
46 L.F. Mollenauer and S. Pan, *Phys.Rev. B*, 1972, **6**, 772.
47 D.M. Hofmann, B.K. Meyer, F. Lohse, and J.-M. Spaeth, *Phys.Rev.Lett.*, 1984, **53**, 1187.
48 D.M. Hofmann, Dissertation, Paderborn, 1987.
49 F. Lohse, M. Fockele, and J.-M. Spaeth, Proc. 5th Europhysical Topical Conf., 'Lattice Defects in Ionic Crystals, Madrid, 1985.
50 M. Fockele, F. Lohse, J.-M. Spaeth, and R.H. Bartram, Proc. 11th Internat. Conf. on Defects in Insulating Crystals, Parma, Italy, 1988.
51 M. Jordan, H. Sothe, J.-M. Spaeth, and F. Lüty, Proc. 11th Internat. Conf. on Defects in Insulating Crystals, Parma, Italy, 1988.
52 F.J. Ahlers, F. Lohse, J.-M. Spaeth, and L.F. Mollenauer, *Phys.Rev. B*, 1983, **28**, 1249.
53 M. Heinemann, B.K. Meyer, J.-M. Spaeth, and K. Löhnert, in 'Defect Recognition and Image Processing in III-V Compounds II,' ed. E.R. Weber, Elsevier, Amsterdam, 1987.
54 K.P. Dinse and C.J. Winscon, 'Optically detected ENDOR Spectroscopy,' in 'Triplet State ODMR Spectroscopy,' ed. R.H. Clarke, Wiley, New York, 1984.
55 G. Strauch, Th. Vetter, and A. Winnacker, *Phys.Lett.*, 1983, **34**, 160.
56 Y.Sano, K. Morigatei, and I. Hirabayashi, *Physica*, 1983, **117A,118B**, 923.
57 F. Boulitrop, *Phys.Rev. B*, 1983, **28**, 6192.
58 J.J. Davis, J.E. Nichols, and R.P. Barnard, *J.Phys. C*, 1985, **18**, L93.
59 D. Block, A. Hervé, and R.T. Cox, *Phys.Rev. B*, 1982, **25**, 6049.